Nanoscale

PAPER

View Article Online
View Journal | View Issue

Cite this: *Nanoscale*, 2021, **13**, 14879

Cetuximab-Ag_2S quantum dots for fluorescence imaging and highly effective combination of ALA-based photodynamic/chemo-therapy of colorectal cancer cells†

Mahshid Hashemkhani,[a] Gozde Demirci,[a] Ali Bayir,[a] Abdullah Muti,[b] Alphan Sennaroglu,[a,b,c] Layla Mohammad Hadi,[d] Elnaz Yaghini,[d] Marilena Loizidou,[d] Alexander J. MacRobert*[d] and Havva Yagci Acar*[a,e]

Colorectal cancer (CRC) has a poor prognosis and urgently needs better therapeutic approaches. 5-Aminolevulinic acid (ALA) induced protoporphyrin IX (PpIX) based photodynamic therapy (PDT) is already used in the clinic for several cancers but not yet well investigated for CRC. Currently, systemic administration of ALA offers a limited degree of tumour selectivity, except for intracranial tumours, limiting its wider use in the clinic. The combination of effective ALA-PDT and chemotherapy may provide a promising alternative approach for CRC treatment. Herein, theranostic Ag_2S quantum dots (AS–2MPA) optically trackable in near-infrared (NIR), conjugated with endothelial growth factor receptor (EGFR) targeting Cetuximab (Cet) and loaded with ALA for PDT monotherapy or ALA/5-fluorouracil (5FU) for the combination therapy are proposed for enhanced treatment of EGFR(+) CRC. AS–2MPA–Cet exhibited excellent targeting of the high EGFR expressing cells and showed a strong intracellular signal for NIR optical detection in a comparative study performed on SW480, HCT116, and HT29 cells, which exhibit high, medium and low EGFR expression, respectively. Targeting provided enhanced uptake of the ALA loaded nanoparticles by strong EGFR expressing cells and formation of higher levels of PpIX. Cells also differ in their efficiency to convert ALA to PpIX, and SW480 was the best, followed by HT29, while HCT116 was determined as unsuitable for ALA-PDT. The therapeutic efficacy was evaluated in 2D cell cultures and 3D spheroids of SW480 and HT29 cells using AS–2MPA with either electrostatically loaded, hydrazone or amide linked ALA to achieve different levels of pH or enzyme sensitive release. Most effective phototoxicity was observed in SW480 cells using AS–2MPA–ALA–electrostatic–Cet due to enhanced uptake of the particles, fast ALA release and effective ALA-to-PpIX conversion. Targeted delivery reduced the effective ALA concentration significantly which was further reduced with codelivery of 5FU. Delivery of ALA *via* covalent linkages was also effective for PDT, but required a longer incubation time for the release of ALA in therapeutic doses. Phototoxicity was correlated with high levels of reactive oxygen species (ROS) and apoptotic/necrotic cell death. Hence, both AS–2MPA–ALA–Cet based PDT and AS–2MPA–ALA–Cet–5FU based chemo/PDT combination therapy coupled with strong NIR tracking of the nanoparticles demonstrate an exceptional therapeutic effect on CRC cells and excellent potential for synergistic multistage tumour targeting therapy.

Received 1st June 2021,
Accepted 5th August 2021

DOI: 10.1039/d1nr03507j

rsc.li/nanoscale

Introduction

Colorectal cancer (CRC) is the third-most diagnosed cancer and the fourth leading cause of cancer deaths worldwide.[1,2] Surgical resection is potentially curative at the early-stage; at advanced-stages when the tumour is metastatic or inoperable, patients have a 5% survival rate in 5 years. The most common treatment methods of inoperable cases are radiotherapy and conventional chemotherapy utilising drugs such as 5-fluorouracil (5FU), oxaliplatin, and capecitabine. 5FU is one of the

[a]*Koc University, Graduate School of Materials Science and Engineering, Rumelifeneri Yolu, Sariyer, 34450 Istanbul, Turkey. E-mail: fyagci@ku.edu.tr*
[b]*Koc University, Departments of Physics and Electrical-Electronics Engineering, Rumelifeneri Yolu, Sariyer 34450, Istanbul, Turkey*
[c]*Koc University, KUYTAM, Rumelifeneri Yolu, Sariyer 34450, Istanbul, Turkey*
[d]*Division of Surgery and Interventional Science, Centre for Nanomedicine and Surgical Theranostics, University College London, Royal Free Campus, Rowland Hill St, London NW3 2PE, UK. E-mail: a.macrobert@ucl.ac.uk*
[e]*Koc University, Department of Chemistry, Rumelifeneri Yolu, Sariyer 34450, Istanbul, Turkey*

†Electronic supplementary information (ESI) available. See DOI: 10.1039/d1nr03507j

widely used drugs but suffers from low lipophilicity, non-selective biodistribution, low bioavailability, and various side effects.[3–5] Therefore, the development of highly sensitive detection techniques for early diagnosis and targeted treatments of CRC is an urgent demand in the field.

Light-based therapies are exciting alternative treatment methods that provide high locality. Photodynamic therapy (PDT), which involves photoexcitation of a photosensitiser (PS) at a specific wavelength to generate toxic reactive oxygen species (ROS), is already used in the clinic for the treatment of some cancerous and non-cancerous indications.[6–8] Low dark toxicity of such PSs, presence of a "turn on" mechanism with localised light and a short travel distance of ROS reduce the off-site toxicity while increasing the locality of the treatment.[9] Ability to repeat PDT without cumulative toxicity and its effectiveness in even chemo- and radio-resistant cells are quite attractive features of PDT, which makes PDT a promising single as well as an adjuvant therapy.[9] PDT is mostly used for melanoma, head and neck, pancreatic, and bladder cancers.[5,10,11] There are only a few examples of PDT of CRC.[12–15] In a clinical study performed with 23 patients with advanced CRC, Photofrin II-based PDT effectively reduced complications and hospital stay and increased the survival time.[15] Redaporfin-based PDT of CT29-tumour xenografts caused complete regression of the tumour in 83% of the treated mice.[16] However, PDT has several limitations as well. These include long-term cutaneous photosensitivity, short excitation wavelengths, poor PS solubility/stability, quick clearance, and low tumour selectivity.[11,17] Therefore, selective and high accumulation of the PSs at the tumour site, just like the chemotherapeutic agents, but also solubilisation and stabilisation of the PSs in the circulation are urgent needs of PDT for improved therapeutic outcomes.[16,18]

5-Aminolevulinic acid (ALA)-induced protoporphyrin (PpIX) is now widely used for the PDT of tumours and premalignant lesions.[19,20] FDA approval has been granted for the treatment of actinic keratosis using irradiation with blue light, but red light is more commonly employed for cancers such as basal cell carcinoma.[21] Compared to other PSs, ALA offers lower toxicity, and faster clearance and hence only short-term cutaneous photosensitivity for patients.[20] ALA is a natural precursor of the fluorescent protoporphyrin IX (PpIX) in the heme biosynthetic pathway, where the transient formation of PpIX occurs in mitochondria before its conversion to photoinactive heme by ferrochelatase.[22,23] Exogenous administration of ALA causes accumulation of high levels of PpIX, which can be exploited for PDT and fluorescence imaging due to red luminescence of PpIX.[24,25] ALA is a low molecular weight, highly water soluble zwitterionic molecule which causes rapid body clearance, which reduces the patients' photosensitivity but also causes relatively low bioavailability.[26] This seriously limits its successful application in the clinic especially for the cancers of the peripheral organs. Different approaches have been taken to enhance the bioavailability of ALA such as esterification with long-chain fatty acids to enhance lipophilicity, conjugation to dendrimers, and its loading to liposomes or nanoparticles (NPs).[5,19,27] Xu *et al.* showed that cationic Au nanoparticles with electrostatically loaded ALA provide higher phototoxicity to K562 (chronic myelogenous leukemia) cells than free ALA.[28] Although very limited, there are some promising examples to ALA-PDT of CRC but it was mostly performed with free ALA.[29–32] Chung *et al.* incorporated ALA into methoxy (polyethylene glycol)/chitosan (PEG-chito), and showed a 2-fold increase in PpIX formation compared to free ALA (0.1 mM) that subsequently caused 50% more phototoxicity in CT26 cells after irradiation at 635 nm (1.2 J cm^{-2} light dose).[13] ALA-PDT is mostly performed at 400–420 nm, which corresponds to the intense Soret porphyrin absorption band or 635 nm, which corresponds to the long-wavelength band that is commonly used in clinics.[28,30,33] Despite lower absorption of PpIX at 635 nm, long wavelength has better safety and deeper penetration.

The use of nanocarriers usually enhances the therapeutic outcome by altering the cell penetration pathway of small drugs, but the desired high specificity of the tumour therapy may be achieved with nanocarriers tagged with monoclonal antibodies that selectively bind to tumour-specific biomarkers. There are several examples wherein antibody targeting of PS loaded nanocarriers improves the phototoxicity significantly.[34,35] About 80% of CRC cells overexpress epidermal growth factor receptor (EGFR) and Cetuximab (Cet), which is an immunoglobulin G1 mouse-human chimeric monoclonal IgG1 antibody, binds to the external domain of epidermal growth factor receptor (EGFR) with 10 times higher affinity than the epithelial growth factor.[36] Therefore, Cet is used clinically as a targeted antibody drug for metastatic CRC in combination with chemotherapy and also as tags to deliver nanocarriers to EGFR (+) tumour cells.[34,37–40]

Here, we investigated the use of Cet conjugated Ag_2S quantum dots (QDs) for the delivery of ALA at therapeutic doses to the EGFR(+) CRC. Ag_2S QDs have been shown as non-toxic *in vitro* and *in vivo* due to low solubility,[41–43] and have a strong luminescence in near-infrared (NIR), which is well suited for medical imaging due to deeper tissue penetration and a higher signal-to-background ratio as a result of lower tissue autofluorescence in the NIR range.[44,45] This is more advantageous than red fluorescence of PpIX (exc 405 nm, em 635 nm), which has been exploited for intra-operative fluorescence imaging of tumours[46,47] despite photobleaching.[48,49] Ag_2S QDs have better resistance to photobleaching, allowing longer operational time and can be excited at longer wavelengths to separate the wavelengths for imaging and PDT. Here, anionic Ag_2S QDs coated with 2-mercaptopropionic acid (2MPA) (AS–2MPA), which is one of the most stable and luminescent (39% QY) NIR QDs with excellent cyto-and hemocompatibility, are exploited.[42,50,51]

Herein, we propose the use of Cet conjugated AS–2MPA QDs loaded with ALA and a first-line anticancer drug, 5-fluorouracil (5FU), to achieve tumour-specific, image-guided PDT/chemotherapy combination in EGFR(+) CRC cell lines (Scheme 1). In the design of such theranostic nanoparticles, Cet was conjugated to Ag_2S–2MPA QDs (AS–2MPA) *via* a PEG

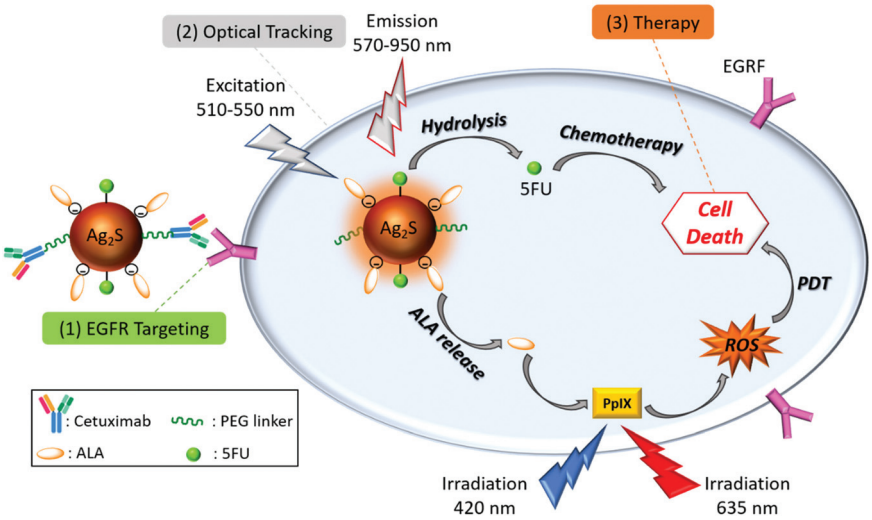

Scheme 1 Design of theranostic nanoparticles for the targeted ALA-PDT monotherapy and combination of PDT/chemotherapy of EGFR(+) CRC cells.

spacer, 5FU was conjugated *via* ester linkages, and ALA was loaded to Ag_2S in three different ways to determine the most efficient approach to produce high levels of PpIX: electrostatically, via pH-sensitive hydrazone linkages or amide bonds. These modes of conjugation were proposed to allow the release of the 5FU and ALA as a response to intrinsic stimuli such as pH, esterase and amidase enzymes and protect them in the physiological pH. This approach will provide: (a) higher tumour accumulation of ALA and 5FU due to active EGFR targeting of the QDs; (b) protection of the ALA and 5FU in the circulation but a selective and rapid release into the acidic tumour microenvironment; (c) increase in the PDT efficiency and locality since PDT is a focal therapy and is effective at the zone which retains sufficient PS and receives sufficient light dose; (d) ability to track the location of QDs due to the strong, stable NIR optical signal in the medical-imaging window along with image-guided therapy option; and finally (e) a synergistic therapeutic effect in the treatment of CRC with the combination of chemotherapy and ALA-based PDT in targeted cells, which would reduce the effective dose of the therapeutic agents.

In the *in vitro* studies, low, intermediate, and high-EGFR overexpressing CRC cell lines, HT29, HCT116, and SW480 cells,[52] were used to confirm the EGFR targeting of Cet conjugated QDs, and their imaging potential. We also investigated the pro-drug incubation time and cell line dependence of ALA to PpIX conversion to elucidate the PDT potential of these cell types. The therapeutic effects of EGFR targeted ALA-PDT monotherapy under both 420 nm and 630 nm irradiation and ALA-PDT/5FU combination therapy of CRC with the designed theranostic QDs were evaluated in both 2D monolayer cell culture and more complex 3D spheroids grown in a compressed collagen matrix, which can replicate a range of physiological features present in the *in vivo* models.[53]

It is worth pointing out that the nanoparticles and the strategy shown here, specifically on colorectal cancer by using 3D models, are indeed adaptable to all EGFR(+) cancers, but also the targeting ligand, as well as the drug, may be changed to adapt these particles and strategy to the targeted combination therapy of other cancers.

Materials and methods

All chemicals were of analytical grade or highest purity. Silver nitrate ($AgNO_3$), *N*-(3-dimethylaminopropyl)-*N*′-ethylcarbodiimide hydrochloride (EDC), sulfo-*N*-hydroxysuccinimide (sulfo-NHS) and 5-fluorouracil were purchased from Sigma–Aldrich. Sodium sulfide (Na_2S) was obtained from Alfa Aesar. 2-Mercaptopropionic acid (2-MPA), acetic acid (CH_3COOH), sodium hydroxide (NaOH), and Erbitux were provided by Merck. 5-Aminolevulinic acid hydrochloride (ALA) was bought from research products international (USA). Heterobifunctional crosslinker NH_2-poly (ethylene glycol)-maleimide (NH_2-PEG-MI) with an average molecular weight of 2 kDa was obtained from Sunbio (Orinda, USA) and a polysulfone filtration membrane (3, 10 and 100 kDa) from Sartorius (Germany). 20 kDa Slide-A-lyzer dialysis cassette, live/dead cell viability, and Alamar Blue reagents were bought from Thermo Fisher Scientific (USA). An Annexin V-FITC early apoptosis detection kit was purchased from Cell Signaling Technology (UK).

Roswell Park Memorial Institute (RPMI) 1640 medium (with L-glutamine and 25 mM HEPES) 1640 and McCoy's 5A (Modified) medium were obtained from Multicell, Wisent Inc. (Canada). Fetal bovine serum was provided by Capricorn Scientific GmbH (Germany). Trypsin–EDTA and penicillin streptomycin solutions were purchased from Wisent Inc. (Canada). Thiazolyl blue tetrazolium bromide (MTT) and phosphate buffered saline (PBS) tablets were purchased from Biomatik Corp. 80% Rat Tail Collagen Type I was bought from

First Link UK Ltd. Paraformaldehyde solution 4% in PBS was obtained from Santa Cruz Biotechnology, Inc. (USA). 96-Well plates were purchased from Nest Biotechnology Co. Ltd (China). Human breast adenocarcinoma cells (HT29 and SW480) were given as a gift by the Gozuacik Lab (Sabanci University, Istanbul, Turkey) for this study. HCT116 cells were purchased from ATCC (Ireland).

Synthesis of AS–2MPA QDs

2MPA coated AS (AS–2MPA) QDs were prepared as described in the literature.[42] As an example, 110 μL of 2MPA was dissolved in 75 mL of deoxygenated water in a round-bottomed flask under argon, and then the pH of the solution was adjusted to 7.5 using NaOH and CH_3COOH (1 M). 42.5 mg of $AgNO_3$ was added to this solution, and the pH was adjusted to 7.5 again. Here, 4.9 mg of Na_2S for an Ag/S molar ratio of 4/1 was dissolved in 25 mL of deoxygenated water, separately and added gently to the initial solution under vigorous mechanical stirring (500 rpm) for 90 min at room temperature (RT). QD solutions were washed with de-ionised water using Sartorius centrifugal filters (3 kDa cut-off) to remove excess unreacted molecules and stored in the dark at 4 °C.

Synthesis of AS–2MPA–ALA

In all three different ways of ALA loading, 25 mg of AS–2MPA (8.5 mg mL^{-1}) and ALA in an amount corresponding to 30 mol% (0.044 mmol) of the 2MPA content of the AS–2MPA QDs determined by TGA analysis (Fig. S1a†) was used.

Electrostatic loading of ALA to AS–2MPA (AS–2MPA–ALA–electrostatic)

ALA was dissolved in HEPES (pH: 7.2–7.4) and filtered using a 0.2 μm sterile filter and then was mixed with AS–2MPA in HEPES at RT for 30 min (Scheme S1a†). Loading was performed freshly before cell studies and the solution was kept in the dark at 4 °C until use.

Electrostatic loading was confirmed with Isothermal titration calorimetry (Affinity ITC, USA). AS–2MPA QDs (1 mL, 1 mg mL^{-1} in HEPES) were titrated with ALA (total of 250 μl from 3 mg mL^{-1} in HEPES) at a rate of 5 μL s^{-1} at 25 °C. Strong binding exotherms observed throughout the titration (Fig. S1b†) confirmed complete binding of ALA to QDs electrostatically. Therefore, after the electrostatic loading of ALA, no washing was performed.

Conjugation of ALA to AS–2MPA *via* hydrazone linkage (AS–2MPA–ALA–ADH)

Adipic acid dihydrazide (ADH) (9.5 mg) was added to AS–2MPA in DI water. The pH of the reaction mixture was adjusted to 6 by addition of 1 M CH_3COOH/NaOH. EDC (0.09 mmol) in 1 mL of MES buffer (pH = 6, 0.1 M) was added to the reaction mixture and mixed at RT for 2 h. The solution was washed with DI water using centrifugal filters (3 kDa cut-off), and then the pH of the solution was adjusted to 8–9 by adding 1 M NaOH. ALA dissolved in 1 mL water was added to this solution and left stirring overnight at RT (Scheme S1b†). Finally, the prepared QD solutions were washed with DI water using centrifugal filters (3 kDa cut-off) and stored in the dark at 4 °C. The amount of unbound ALA was calculated from its absorbance at 263 nm using a concentration-dependent absorbance calibration curve for ALA. The bound amount was calculated accordingly.

Direct conjugation of ALA to AS–2MPA QDs *via* amidation (AS–2MPA–ALA–amide)

First, EDC (0.088 mmol) and 5 min later sulfo-NHS (then 0.088 mmol) were added to AS–2MPA in MES buffer (pH = 6, 0.1 M), and the mixture was stirred for 30 min at RT. Then, ALA was added to the solution of activated QDs, and the mixture was kept stirring overnight for amidation (Scheme S1c†). Finally, QD solutions were washed with DI water using centrifugal filters (3 kDa cut-off) and stored in the dark at 4 °C. The amount of unconjugated ALA was calculated as described above.

Conjugation of Cet to AS–2MPA QDs

NH_2-PEG-MI was used as a bridge between the Cet and QDs. AS–2MPA QDs in MES buffer (pH 6) were activated with 14.6×10^{-4} mmol of EDC and sulfo-NHS as described above. Then, the medium was exchanged with PBS (1×, pH = 7.2–7.4) and 14.6×10^{-6} mmol NH_2-PEG-MI (2 kDa) in 1 mL PBS buffer was added to the reaction solution. After overnight reaction under mild stirring at RT, QDs were washed with PBS through a 3 kDa cut-off ultracentrifuge tube (Scheme S2†).

Cet was thiolated to react with maleimide (MI) of the PEG bridge *via* the thiol–ene reaction. For thiolation, Cet (3 mg mL^{-1} in PBS) was incubated with 21.75×10^{-4} mmol of 2-iminothiolane solutions (Traut's reagent, 1 mg mL^{-1} PBS-EDTA, pH = 8) for 2 h at RT and then dialysed in a 20 kDa dialysis cassette in phosphate buffer-EDTA (pH = 8) for 5–6 h. Freshly prepared thiolated-Cet (Cet-SH) was added to the QD solutions (in PBS, pH = 7.2–7.4) and stirred overnight at RT. The molar ratio of Cet-SH : NH_2-PEG-MI was 1 : 1. Unbound Cet-SH was removed by washing 6 times with PBS through a 100 kDa cut-off Sartorius centrifugal filter.

The amount of Cet conjugated to the QDs was calculated according to the Bradford assay. Briefly, bovine serum albumin protein at 0, 1, 2, 4, 6, 8, 10, and 20 μg mL^{-1} concentrations in PBS was used as a standard. The washed product of AS–2MPA–Cet was concentrated and measured as the analyte. 1 ml of each reference and analyte were mixed with 1 mL of Bradford reagent for 10 min at RT. Then, the absorbance at 595 nm was recorded using ultraviolet-visible (UV-vis) spectroscopy.

Synthesis of AS–2MPA–Cet–ALA

ALA was electrostatically loaded to AS–2MPA–Cet as described above for AS–2MPA–ALA–electrostatic.

In the case of amide and hydrazone linked ALA on Cet conjugated QDs, ALA conjugation was performed after H_2N–PEG–MI conjugation to AS–2MPA, following the procedures described above. Cet conjugation was performed as the final

step of the nanoparticle synthesis *via* the thiol–ene method detailed above, to protect the antibody.

Synthesis of AS–2MPA–ALA–Cet–5FU

First, 5FU was reacted with formaldehyde at 60 °C in an oil bath for 4 h to produce 5FU-diol (Scheme S3†).[54] QDs in water were protonated with dropwise addition of acetic acid and precipitated with centrifugation. Isolated QDs were suspended in dry DMF. For the esterification reaction, 50 mg QDs in DMF (5 mg mL^{-1}), 10.74 mg 5FU-diol and 2.3 mg DMAP were added and stirred at RT. After the reaction flask was cooled down in an ice bath, 11.66 mg DCC was added to the reaction mixture and stirred overnight under Ar flow. Dichloromethane was added and 5FU conjugated QDs were extracted into the aqueous phase. AS–2MPA–5FU QDs were washed with DI water from 3 kDa centrifugal filters. The amount of the unconjugated 5FU present in the filtrate was quantified from the absorbance of 5FU at 279 nm by using a concentration-dependent absorbance calibration curve of 5FU. The conjugated 5FU amount was determined as 15 mol% of 2MPA content of the QDs.

Cet was conjugated to AS–2MPA–5FU, and then ALA was electrostatically loaded following the procedures given above for each of these steps.

Characterisation

The absorbance was measured using a Shimadzu UV-3600 spectrophotometer in the 300–1000 nm range. The crystal sizes of AS were calculated using the Brus equation:[55]

$$\Delta E = \frac{\hbar^2\pi^2}{8R^2}\left[\frac{1}{m_e}+\frac{1}{m_h}\right] - 1.8\frac{e^2}{\varepsilon_{Ag_2S}4\pi\varepsilon_0 R},$$

where ΔE is the band gap energy difference, m_e ($0.286m_0$) and m_h (1.096) are the respective effective electron and hole masses for AS, ε_{AS} (5.95) is the dielectric constant of bulk AS and R is the radius of the nanocrystal.

To measure the photoluminescence (PL) intensity, a home-made instrument with a femtowatt sensitive Si detector (Thorlabs PDF10A, 1.4×10^{-15} W $Hz^{-1/2}$) and a 1/8 Newport Cornerstone 130 monochromator having 600 L mm^{-1} grating was used over the wavelength range of 600–1100 nm. AS–2MPA QDs were excited with a frequency-doubled output of a DPSS laser operating at 532 nm excitation wavelength. The luminescence signal was filtered using a 590 nm long-pass filter.

Hydrodynamic size, zeta potential, and polydispersity index (PDI) measurements of the aqueous QDs were performed using a Malvern zetasizer nano ZS. The Ag^+ content of the QD solutions was employed after treating samples with sulfuric acid (96%) and nitric acid (65%) (at a ratio of 1 : 9 v/v) using an Agilent 7700x Inductively Coupled Plasma Mass Spectrometer (ICP-MS).

ALA release

The release of ALA from QDs was investigated at different pH values (pH 5.5 and 7.4). Typically, AS–2MPA–ALA–electrostatic, AS–2MPA–ADH, and AS–2MPA–amide QDs (5 mL) were added to a dialysis bag (MWCO 3500) and then immersed in 500 mL of PBS (pH 5.5 and 7.4) under constant shaking (150 rpm) at 37 °C. At fixed time intervals, 3 mL of the solution was taken out, and 3 mL fresh PBS medium was added. The amount of ALA in each aliquot was calculated from its absorbance at 263 nm using a concentration-dependent standard curve prepared for ALA in PBS at (pH 5.5 and 7.4).

Cell culture

Different EGFR overexpressing human colon adenocarcinoma cells (HT29: low, HCT116: intermediate, and SW480: high) and healthy colorectal cells (CCD481) were cultured in complete McCoy's, MEM, and DMEM media supplemented with 10% fetal bovine serum and 1% penicillin–streptomycin antibiotic solution according to ATCC recommendations.[52] Trypsin-EDTA was used for the detachment of the cells.

Preparation of 3D cancer spheroids

The 3D *in vitro* cancer spheroids grown in a compressed type I collagen hydrogel were prepared following the protocol from RAFT 3D culture systems (Lonza, Slough, UK).[56] Compressed type I collagen gels have a much higher density of collagen (*c.* 10% wt/vol) compared to standard hydrogels (<0.5% wt/vol), and therefore enable better cellular interaction with the extracellular matrix to be replicated. The lower rate of oxygen diffusion through higher density hydrogels is also relevant to PDT since it is reliant on an adequate supply of oxygen, which cannot be replicated in monolayer cultures.

The hydrogels were prepared from a mixture containing 10% 10× MEM (used as the colour/pH indicator) and 80% Rat Tail Collagen Type I (First Link UK Ltd Custom Bio-Reagents) before undergoing neutralisation using a solution made from 1.65 M NaOH and 840 mM HEPES buffer solution (Thermo Fisher Scientific). The cells were seeded into the collagen at a density of 50 000 cells for spheroids at an overall mixture volume of 240 μL per well in a 96-well plate. The spheroids were incubated at 37 °C for 15 min to set before being subjected to plastic compression using absorbers (Lonza) at RT for a further 15 min. After the removal of the absorbers, fresh medium was added, and the spheroids were placed in the incubator.

Determination of cellular viability

Viability was evaluated by performing the thiazolyl blue tetrazolium bromide (3-(4,5-dimethyl-thiazol-2yl)-2,5-diphenyltetrazolium bromide, MTT) and Alamar blue assays on HCT116, HT29, and SW480 cell lines before/after PDT. Cells were seeded at a density of 12 500 cells per well into 96-well culture plates in culture medium and incubated under a 37 °C and 5% CO_2 atmosphere for 24 h. Following incubation, the medium was replenished; cells were treated with QDs (25–500 μg mL^{-1} [Ag]) and incubated for 48 h. Then, the medium was removed, and cells were washed with PBS. MTT reaction solution was added to the cells and incubated for 4 more hours. DMSO–ethanol (1 : 1 v/v) solution (200 μL) was

added into the wells and plates were shaken gently for 15 min to dissolve the purple formazan formed as a result of the mitochondrial activity of the viable cells. Absorbances at 600 nm and 640 nm were measured in each well with a Bio-Tek EL × 800 Absorbance Microplate Reader, and the reference absorbance at 640 nm was subtracted from the absorbance at 600 nm. To decouple any interaction between the QDs and the MTT reagents, QDs were treated with the MTT protocol, and the measured absorbance was subtracted from the formazan values.

The absorbance-based MTT assay cannot be used for light scattering 3D culture models; hence the fluorescence-based Alamar blue assay was used for the viability testing in 3D spheroids grown within a compressed collagen matrix. For this, the cells were seeded, and the QDs were added as described for the MTT assay. After the specific incubation time, cells were washed and then incubated with the Alamar blue solution (10% v/v Alamar blue in fresh medium) for 2 h and the solutions were transferred from each well into a black 96-well plate (TPP, Sigma Aldrich, UK) for measurements. The fluorescence intensities of each well were measured at 590 nm with 530 nm excitation using a Fluoroskan ascent FL plate reader (Thermo Labsystems, UK).

Cell uptake

Qualitative analysis. The *in vitro* cell imaging of QDs was performed on the 2D culture first using a confocal microscope (Leica dmi8/SP8) to show the cell uptake qualitatively. HCT116, SW480, and HT29 cells were grown on 3 mL glass-bottom Petri dishes at a density of 1.5×10^5 cells per well in complete medium and incubated at 37 °C under 5% CO_2 for 24 h. QDs at 100 μg mL^{-1} [Ag] were introduced into the cells, and after 4 and 24 h incubation, the cells were washed three times with PBS to remove uninternalised QDs. Then, the cells were fixed with paraformaldehyde solution (4% in PBS) for 20 min. Cells were incubated for an additional 15 min with 2 μg mL^{-1} of DAPI, a nuclear staining dye. The cells were rewashed with PBS three times to remove the unbound dye and 1 mL PBS was left in each well to protect the cells against drying.

The fixed cell samples were examined using a confocal microscope (Leica dmi8/SP8) with two different filters for the NIR region (λ_{exc}: 510–550 nm and λ_{em}: 710 nm long pass) and DAPI (λ_{exc}: 325–375 nm and λ_{em}: 435–485 nm). The same experimental procedure was also performed for control cells which were not treated with QDs. Images were processed and merged using the ImageJ analysis program.

Quantitative analysis. The quantitative analysis of QD uptake was performed by the determination of Ag content in the QD treated cells. HCT116, SW480, and HT29 cells were seeded on a 12-well plate at a density of 1.5×10^5 cells per well complete medium and grown for 24 h at 37 °C and 5% CO_2. Next day, the growing cells were incubated with QD samples at 100 μg mL^{-1} [Ag] for 4 and 24 h. Then, the cells were washed with PBS to remove uninternalised QDs and were collected after being trypsinised. Cells were digested with acid (HNO_3/H_2SO_4: 9/1 v/v) for about 1 week at RT, and Ag content was determined by ICP-MS ($n = 3$).

Imaging 3D spheroids. The multicellular aggregates of HT29 and SW480 (50 000 cells per model) were grown for 7 days. Then, the spheroids were incubated with QDs at 100 μg mL^{-1} [Ag] for 4 and 24 h. The spheroids were washed three times with PBS and incubated with PBS for imaging with an Olympus fluorescence microscope (10× objective, Olympus BX63) with the following bandpass filters: BF (λ_{exc}: 345 nm and λ_{em}: 455), CY8 (λ_{exc}: 480 nm and λ_{em}: 810 nm) and TRITC (λ_{exc}: 545 nm and λ_{em}: 580–650 nm (band pass filter). The spheroids without QD treatment were used as controls.

Measurement of PpIX formation

HCT116, SW480, and HT29 cells were seeded as described in the cytotoxicity study. After 24 h of incubation, the medium was replaced with a serum-free medium to prevent efflux of PpIX mediated by binding to serum proteins, and PpIX fluorescence from each well was measured at 635 nm every 2 h (excitation at 420 nm; Synergy H1 microplate reader (Biotek)). Untreated cells were used as the control.

PDT studies

For the *in vitro* PDT studies, HCT116, SW480, and HT29 cells at a density of 12 500 cells per well (2D cell culture) and 50 000 cells per well (3D models) were seeded in 96-well plates and cultured as described above for 24 h (2D cell culture) or 7 days (3D models). Cells were treated with QDs between 25 and 100 μg mL^{-1} Ag concentrations or with free ALA (0.17–0.7 mM) for 4 and 24 h. Then, the medium was replenished with serum-free medium, and each well was illuminated with either a blue flatbed lamp with peak emission at 420 nm (7 mW cm^{-2}, 2.1 J cm^{-2}) (Lumisource, PCI Biotech, Oslo, Norway) for 5 min or a 640 nm laser for 1 min from the bottom of the plate. The output beam of the 640 nm laser was adjusted with the help of a telescope to match the beam diameter to the diameter of the wells on the 96-well plate. The diode laser delivered a power of 100 mW, corresponding to an irradiance fluence of 0.26 W cm^{-2}, and a fluence of 15.5 J cm^{-2} after 1 minute exposure. Light irradiated cells were then incubated for further 24 h before cell viability was determined using standard MTT (2D cell culture) or Alamar blue (3D models) assays. Cells that were not treated with QD, free ALA or light were used as a control. Cells that were not treated with QDs or ALA but irradiated were used as a "laser control".

Determination of reactive oxygen species (ROS generation)

HT29 and SW480 cells were treated with QDs at a 100 μg mL^{-1} Ag concentration for 24 h and irradiated either 5 min at 420 nm (7 mW cm^{-2} output power, 2.1 J cm^{-2} fluence) with a LumiSource-flatbed lamp (PCI Biotech, Oslo, Norway) or 1 min at 640 nm with laser (100 mW output power, irradiance fluence of 0.26 W cm^{-2}, and fluence of 15.5 J cm^{-2}) from the bottom of the plate and incubated for further 24 h. The ROS levels in the cells were determined using two different ROS generation kits: (1) the Enzo Total ROS Detection Kit at exci-

tation/emission wavelengths of 485/538 nm for 420 nm irradiation and (2) the Abcam cellular ROS Detection Kit (orange) at excitation/emission: 540/570 nm for 640 nm irradiation following the manufacturer's instructions using a Synergy H1 microplate reader (Biotek).

Live/dead staining

Live/dead cell viability assay was used to determine live and dead cells before and after PDT treatment. SW480 and HT29 cells were treated with QDs for 4 h at 100 μg mL^{-1} [Ag] concentration and irradiated at 420 nm for 5 min or at 640 nm for 1 nm as described above. After 24 h post-irradiation incubation, cells were stained with the dyes of live/dead assay following the manufacturer's protocol. Fluorescence images were collected using a fluorescence microscope (for 2D: Zeiss Axio observer Z1 and for 3D: EVOS FL colour, Life Technologies, Thermo Fisher Scientific, UK).

Detection of apoptosis/necrosis

An Annexin V-FITC apoptosis detection kit (Abcam, UK) was used to confirm the mechanism of cell death in 2D and 3D models. Cell cultures were treated with 100 μg mL^{-1} [Ag] for 24 h, and then irradiated 5 min at 420 nm as described above. Then, 100 μL of 1× Binding buffer was added to each well before adding 1 μL of Annexin V-FITC (ex/em 488/525 nm) and 5 μL of propidium iodide (ex/em 535/617 nm) to the buffer solution in each of the wells. The models were then imaged using an EVOS fluorescence microscope (EVOS FL color, Life Technologies, Thermo Fisher Scientific, UK).

Statistical analysis

Two-way ANOVA with Tukey's multiple comparison test of GraphPad Prism 8 software package was employed for statistical analysis (GraphPad Software, Inc., USA). All data were expressed as mean ± standard deviation (SD), and $p < 0.05$ was considered statistically significant.

Results and discussion

Synthesis and characterisation of AS–2MPA QDs

NIR emitting AS–2MPA QDs were synthesised from $AgNO_3$ and Na_2S using 2MPA as a coating at molar ratios of Ag/S/2MPA of 1/4/5 at RT according to the procedure previously published by our group.[42] AS–2MPA QDs have a strong emission at 830 nm (Fig. 1a). Strong thiol binding on the Ag_2S crystal surface rendered these QDs anionic which also prevented excessive agglomeration due to charge repulsion and provided an effective electrostatic stabilization. The crystal size of the Ag_2S-core was calculated as 2.93 nm using the Brus equation. The hydrodynamic size of the AS–2MPA QDs was measured as ~3/27 nm (number/intensity-based average) by DLS and zeta potential was −35.3 eV (Table 1).

Synthesis and characterisation of AS–2MPA–ALA

ALA was loaded to QDs in three different ways: (1) electrostatically, which is a single step, simple loading approach. Electrostatic interactions are sensitive to pH, which is low in the tumour microenvironment and the endosomal/lysosomal

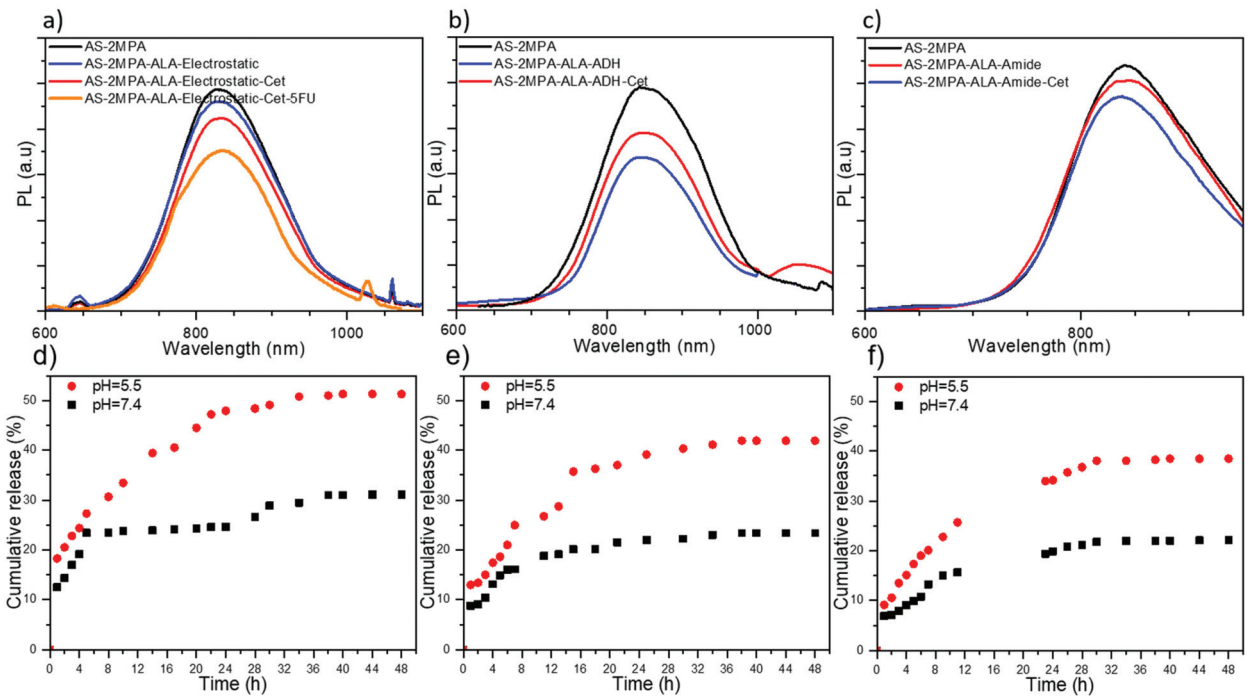

Fig. 1 Photoluminescence spectra of AS–2MPA QDs conjugated with Cet and loaded with ALA *via* (a) electrostatic loading, (b) ADH, and (c) amide bonds. pH-Dependent release profile of ALA from (d) AS–2MPA–ALA–electrostatic, (e) AS–2MPA–ALA–ADH, and (f) AS–2MPA–ALA–amide at 37 °C.

Table 1 Hydrodynamic size, zeta potential and composition of different QD compositions

Name of samples	Dh-number[a] (nm)	Dh-intensity[b] (nm)	Zeta potential (mV)	[Cet] μg mL^{-1}	[ALA] μg mL^{-1}	[Ag] μg mL^{-1}	[5FU] μg mL^{-1}
ALA in HEPES	0.69	5.78	−7.85	—	—	—	—
AS–2MPA in HEPES	5.35	12.98	−7.82	—	—	100	—
AS–2MPA in water	3.03	27.41	−35.30	—	—	100	—
AS–2MPA in PBS	3.61	42.21	−5.81	—	—	100	—
AS–2MPA–ALA–electrostatic[c]	3.53	19.52	−13.60	—	25	100	—
AS–2MPA–ALA–ADH[c]	4.81	118.51	−7.70	—	25	100	—
AS–2MPA–ALA–amide[c]	3.90	112.23	−36.23	—	25	100	—
AS–2MPA–ALA–PEG	6.45	45.11	−7.83	—	25	100	—
AS–2MPA–PEG–Cet[d]	3.31	58.10	−8.87	30	—	100	—
AS–2MPA–ALA–electrostatic–Cet[c]	5.87	49.83	−12.21	30	25	100	—
AS–2MPA–ALA–ADH–Cet[d]	9.19	139.67	−14.26	30	25	100	—
AS–2MPA–ALA–amide–Cet[d]	6.37	147.01	−16.67	30	25	100	—
AS–2MPA–ALA–electrostatic–Cet–5FU[d]	6.27	114.38	−7.78	30	25	100	30

[a] Hydrodynamic diameter measured by DLS and reported as the number average. [b] Hydrodynamic diameter measured by DLS and reported as the intensity average. [c] Particles are in HEPES buffer. [d] Particles are in PBS (pH = 7.4).

compartments of the cells, providing an intrinsic stimulus for the release of ALA; (2) *via* a pH-sensitive hydrazone linkage, which should protect the ALA in the circulation but quickly cleave in the low pH areas; and (3) *via* an amide bond, which is relatively stable under physiological conditions and hydrolyses slowly but preferentially in the acidic environment of the tumour. In ALA loading, 30% of the surface –COOH groups of the AS–2MPA was targeted to have enough functional groups for Cet and 5FU conjugation on the same QD.

Electrostatic loading of ALA to AS–2MPA (AS–2MPA–ALA–electrostatic). Zwitterionic ALA has pK_a values of 4.05 and 8.9. At pH 7.2–7.4, the amine group of ALA is protonated, and the electrostatic interaction between the NH_3^+ group of ALA and COO^- groups of QDs could allow the electrostatic loading of ALA to the QDs[28] (Scheme S1a†). The intensity-based hydrodynamic size of the AS–2MPA QDs changed from 12.98 to 19.52 nm in HEPES buffer (pH = 7.2–7.4) after loading of 30 mol% ALA (Table 1) and the zeta potential increased from −7.82 mV (AS–2MPA in HEPES) to −13.60 mV (AS–2MPA–ALA–electrostatic) confirming the successful electrostatic loading of ALA. Free carboxylic acid groups of ALA may facilitate an increase in the negative charge of the QDs at pH 7.4. Furthermore, the emission spectra of QDs showed a slight red shift and less than *ca.* 10% luminescence reduction after ALA loading. Reduction in the emission intensity is typical when QDs are subjected to post-synthetic modifications due to changes in the medium and the surface of QDs.

Covalent conjugation of ALA to AS–2MPA (AS–2MPA–ALA–ADH and AS–2MPA–ALA–amide). Conjugation of ALA to QDs *via* acid-labile hydrazone linkage was performed by using an adipic dihydrazide linker which was first conjugated to QDs *via* amidation, and then to ALA (Scheme S1b†). Conjugation efficiency was about 70%, which means that 28 mol% of surface carboxylic acid groups of AS–2MPA were conjugated with ALA. These particles (AS–2MPA–ALA–ADH) have a relatively low zeta potential (−7.70 mV) since –COOH groups were replaced with zwitterionic ALA. Particles were also aggregated slightly indicated by a larger hydrodynamic size (118.51 nm), but still, the number-based average was 4.81 nm. There is about 20% reduction in the PL intensity with respect to AS–2MPA, but QDs still have strong luminescence (Fig. 1b).

ALA was also conjugated to QDs *via* an amide linkage utilising the well-known activated ester chemistry (Scheme S1c†). AS–2MPA–ALA–amide QDs have 26 mol% ALA with respect to their 2MPA content. Their hydrodynamic size was similar to that of hydrazone linked ones (112.23 nm), suggesting some aggregation, but not dramatic since the number-based average was again small (3.90 nm). The charge of the AS–2MPA–ALA–amide QDs was similar to that of AS–2MPA (−35.30 and −36.23 mV). This is reasonable since the amine group of ALA was used for conjugation, and its carboxylic acid groups substitute the lost –COOH from the surface of the QDs. The PL and absorbance spectra remain almost unchanged after the conjugation with only 7% reduction in PL intensity (Fig. 1c and Fig. S2c†). Overall, the emission wavelength did not change significantly, but a typical small loss in the intensity was observed after ALA was loaded or conjugated to QDs.

Synthesis and characterisation of EGFR targeting QDs (AS–2MPA–ALA–Cet)

Cet was conjugated to 0.01 mol% of the carboxylic acid groups of AS–2MPA *via* a PEG spacer to increase the accessibility of Cet to EGFRs. A three-step protocol was followed to synthesise QDs bearing both Cet and covalently linked ALA: first, NH_2-PEG-MI (MW 2000 Da) was conjugated to QDs *via* amidation, then ALA was conjugated to QDs, and in the last step thiolated Cet was conjugated to QDs *via* thiol–ene chemistry (Scheme S2†). In the case of electrostatically loaded ALA, first Cet conjugated QDs were prepared (Scheme S2†), and then ALA was loaded. The efficiency of antibody conjugation to QDs was determined as 94–97% by Bradford assay. As shown in Table 1, Cet conjugation increases the hydrodynamic size of the ALA loaded QDs, slightly. The smallest one was again the ALA loaded one (50 nm) and the ADH and amide linked ones were larger (140–150 nm), with a negative surface charge (*ca.* −12 to −17 mV). But, the number based average sizes are

again 6–9 nm. Overall, these particles are small enough to study targeted delivery of cargo exploiting by receptor-mediated internalisation of Cet conjugated QDs. The impact of Cet conjugation on luminescence was again a small drop with respect to AS–2MPA QDs in an amount of 12, 20, and 13% in the case of AS–2MPA–ALA–electrostatic–Cet, AS–2MPA–ALA–ADH–Cet, and AS–2MPA–ALA–amide–Cet QDs, respectively (Fig. 1).

Long term stability of AS–2MPA up to 6 months was studied previously with no loss of emission or colloidal stability.[42] Here, no loss of colloidal stability was observed for over a year, as well. On the other hand, emission intensity decreases by about 25–40% after 20 days (Fig. S3†) when QDs underwent chemical modification on the surface, which is probably due to surface perturbations and defects that occurred during the chemical modifications. Yet, these QDs still have strong enough emission to be exploited as confirmed by their strong intracellular optical signals shown in later sections. Furthermore, Table S2† shows that the hydrodynamic size of the particles usually increased slightly with an increasing size distribution, especially in Cet conjugated compositions, which may also contribute to a slight loss in emission intensity. However, the sizes of QD compositions are small enough to allow receptor targeting in the *in vitro* 2D and 3D experiments, as demonstrated in later sections.

Cetuximab conjugated QDs for simultaneous delivery of ALA and 5FU (AS–2MPA–ALA–Cet–5FU)

In the case of the QDs designed for targeted chemotherapy and PDT combination, only electrostatic loading of ALA was studied. 5FU was conjugated to AS–2MPA QDs *via* ester bonds with 50% efficiency producing particles with 15 mol% 5FU with respect to carboxylic acid groups of the QDs. Then, Cet was conjugated (0.01 mol%) followed by ALA's electrostatic loading (30 mol%) (Scheme S3). The emission peak position of these AS–2MPA–ALA–electrostatic–Cet–5FU QDs did not shift, but the intensity was reduced about 30% with respect to AS–2MPA (Fig. 1a), which was accompanied by an increase in the hydrodynamic size from 49.8 to 114.4 nm with an expected drop in the zeta potential since –COOH groups were consumed (Table 1). Overall, the proposed EGFR targeting AS-QDs delivering 5FU and ALA were successfully synthesised in small sizes with strong emission at about 830 nm.

ALA release from QDs

Conjugation of ALA to the QDs is designed to restrict its release at physiological pH, but promote it in the acidic micro-environment of the tumour and within the endosome/lysosomes. Therefore, the release rate of ALA in PBS at pH 5.5 and 7.4 from all three ALA loaded/conjugated QDs was monitored for 48 h at 37 °C. Protonation of carboxylic acids at acidic pH would weaken the electrostatic interaction between ALA and anionic QDs, resulting in its release over time. Electrostatically loaded ALA showed about 18% initial burst release from QDs at pH 5.5 followed by sustained release reaching about 50% at 32 h (Fig. 1d). At pH 7.4, the initial release was 12%, reaching a plateau at 24% in about 4 h and finally to 30% in 32 h. These data represent adequate protection in the circulation with an enhanced release under acidic conditions.

In AS–2MPA–ALA–ADH QDs, the initial burst release was lower at both pH values (Fig. 1e). Total ALA release at neutral pH was only 19% within 12 h, but was *ca.* 30% at pH 5.5 due to acid hydrolysis of the hydrazone bond. A plateau was reached after 30 h at *ca.* 42% and 24% release at pH 5.5 and 7.4. ALA release from AS–2MPA–ALA–amide QDs was the slowest as expected since the amide bond is the strongest bond used here at both pH values. In 24 h, 22% and 34% ALA were released at pH 7.4 to 5.5, respectively, but in 4 h the release was about 13 and 8% at acidic and neutral pH. This pH-dependent ALA release is very desirable for cancer therapy since it minimises the amount of drug release during blood circulation while it introduces a sufficient amount of drug inside cancer cells.

Overall, as shown in Fig. 1d–f, the ALA release at pH 5.5 after 4 h was 25, 18, and 15 and after 24 h was 48, 39, and 34% from AS–2MPA–ALA–electrostatic, AS–2MPA–ALA–ADH and AS–2MPA–ALA–amide QDs, respectively. The release is faster from the electrostatically loaded QDs and slower with the co-valently conjugated ones, which slow down with the increasing stability of the bonds. This is indeed in agreement with the literature. Sangtani *et al.* observed significant intracellular release of Doxorubicin (DOX) conjugated to CdSe/ZnS QDs *via* an ester linkage but not from amide or hydrazone linked ones in a 2 h incubation period.[57] Release from hydrazone linked DOX started to be seen after an 8 h incubation time. Despite many publications reporting much faster DOX release from hydrazone linked matrices, the slower hydrolysis in their case was attributed to the nanoparticle itself. Indeed, we do think that proximity to the nanoparticle surface may cause some steric hindrance which was suggested as a slowing factor in the hydrolysis rate of ester and amide bonded ALA by Zhu *et al.*[58] Studies in the literature also point to the fact that the kinetics of ester, amide, and hydrazone bond cleavages relies on the environment, sterics, lipophilicity and the cell type. Overall, these results demonstrate that all three conjugation methods could be tested for ALA-based PDT.

Evaluation of EGFR targeting

EGFR targeting ability of Cet conjugated QDs was examined in three different cell lines with different EGFR expression levels. HT29, HCT116, and SW480 cell lines are low, intermediate, and high EGFR expressing cell lines, respectively. The internalisation of QDs by these three cell lines was determined qualitatively by fluorescence microscopy and quantitatively by ICP-MS after 4 and 24 h incubation of cells with QDs at 100 μg mL^{-1} [Ag] dose (Fig. 2). Short incubation times were used to differentiate receptor-mediated endocytosis from the passive endocytic uptake of QDs by the cancer cells. According to ICP, which quantified the internalised QDs based on intracellular Ag concentration, none of these three cell lines differentiated the AS–2MPA from the AS–2MPA–ALA family after 4 h incubation, indicating that ALA loading by either method did not

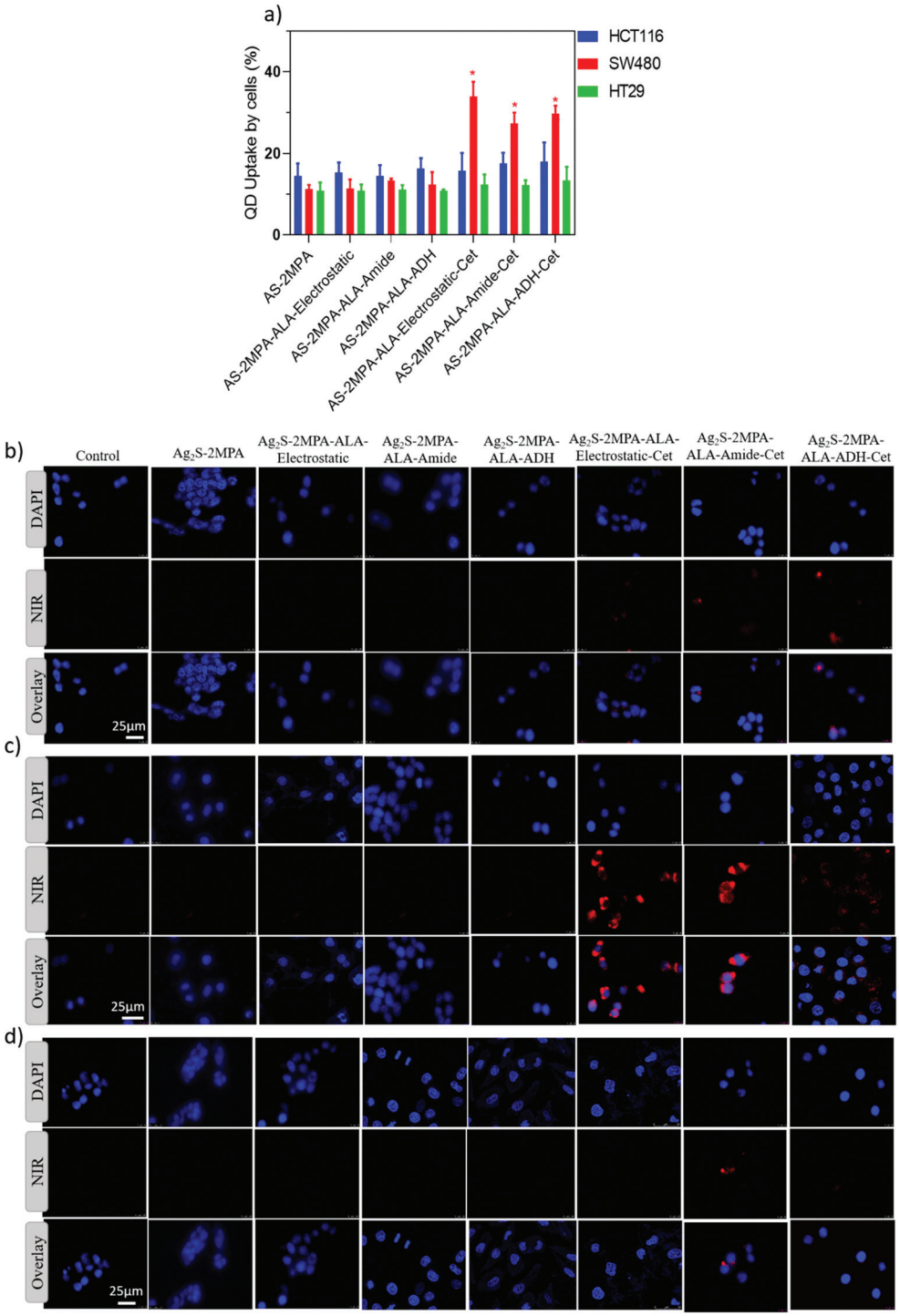

Fig. 2 (a) Intracellular quantification of QDs in HCT116, SW480, and HT29 cells treated with QDs at 100 μg mL^{-1} [Ag] concentration for 4 h. Quantification was based on intracellular Ag concentration determined by ICP-MS. The data are expressed as mean ± S.D. (n = 3), (p < 0.05). Fluorescence microscopy images of (b) HCT116, (c) SW480, and (d) HT29 cells incubated with different conjugates of AS–2MPA QDs for 4 h and untreated control cells. red: luminescence from QDs (excitation/emission: 510–550/710 nm long-pass filter), blue: nuclear stain (excitation/emission: 325–375/435–485 nm). The scale bar = 25 μm.

affect the passive, non-specific endocytosis of the QDs (Fig. 2a). Considering the comparable hydrodynamic sizes (number based) smaller than 10 nm and anionic surface charge, no significant difference in passive endocytosis is expected since only dramatic changes in size and/or charge could affect the passive uptake of nanoparticles.[59] On the other hand, SW480 cells accumulated 2–3 fold more AS–2MPA–ALA–Cet than HT29 and HCT116 cells but again did not

differentiate the Cet conjugated QDs in terms of ALA-loading chemistry. All of the Cet conjugated ALA delivering QDs also have comparable sizes (less than 10 nm) and charges (−12 to −17 mV). Hence, the significantly enhanced uptake of all Cet conjugated particles by only SW480 cells points out fast active transport of QDs *via* EGFR-mediated endocytosis of QDs favoured by the strong EGFR expression level. Binding of Cet to the extracellular domain of the EGFR, which is an internalizing receptor, triggers endocytosis of the QDs and enables active and selective transport of the QDs across the targeted cell membrane.[59,60] This is in agreement with the fluorescence microscopy images of QD treated cells after 4 h incubation. SW480 cells show a strong intracellular optical signal of QDs, while there are only a couple of luminescent cells in HCT116 and HT29 cell lines (Fig. 2b–d).

After 24 h incubation, passive uptake of all QDs by all three CRC cell lines regardless of their EGFR-expression level was observed, as expected, since a significant amount of passive endocytosis also takes place in long incubations (Fig. S4a–c†). Collectively, these data indicate that Cet conjugation enables targeted delivery of QDs selectively to high EGFR-overexpressing SW480 cells. Therefore, there is a strong possibility to deliver high amounts of the pro-drug ALA specifically to high EGFR-expressing cancer cell lines in a short time and detect a collection of the QDs at the tumour site *via* optical imaging in the NIR, followed up by image-guided irradiation of the highlighted tissue.

Evaluation of *in vitro* dark toxicity of AS–2MPA conjugates

The dark toxicity of all QDs produced herein on all three CRC cell lines was evaluated by MTT and Alamar blue viability assays after 48 h incubation of QDs with the cells. The viability of a healthy colorectal cell line (CCD481) treated with these QDs was also determined to compare the selective cytotoxic activity of QDs to CRC cell lines. The dose-dependent toxicity was studied in the range of 25–500 μg mL^{-1} based on the Ag content of different QDs, which was determined by ICP-MS, to keep the number of particles constant for each composition (Fig. S5 and S6†).

Considering the viability above 80% as non-toxic based on ISO 10993-5, ALA, AS–2MPA, and all three different AS–2MPA–ALA compositions exhibited no significant cytotoxicity up to 300 μg mL^{-1} [Ag] based on MTT assay (Fig. 3 and Fig. S5†). Furthermore, the *in vitro* cytotoxicity of all groups of QDs was dose-dependent on each cell line. Cet conjugation to QDs enhanced the cytotoxicity and showed dose-dependence and a more potent anticancer effect on SW480 cell lines than HCT116 and HT29. Viability of Cet conjugated QDs dropped

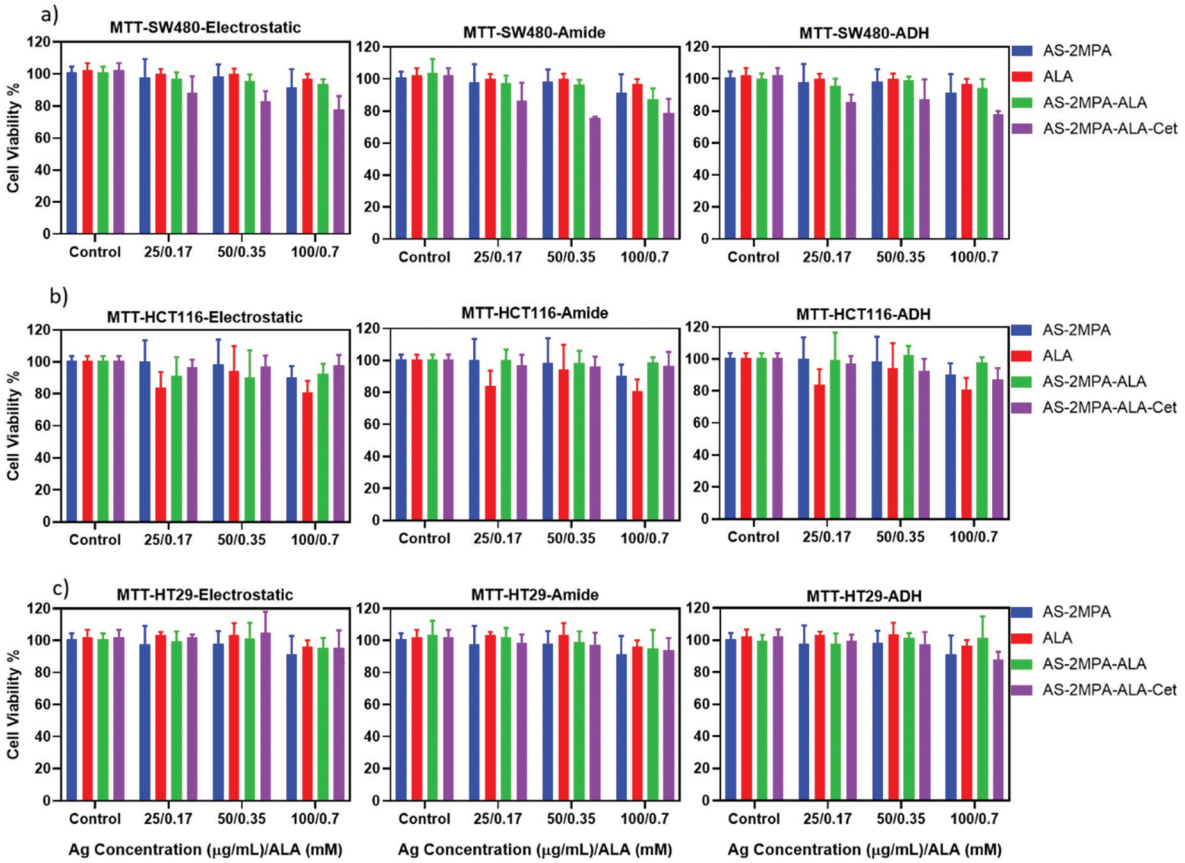

Fig. 3 Viability of (a) HCT116, (b) SW480, and (c) HT29 cells treated with AS–2MPA conjugates at 25–100 μg mL^{-1} [Ag] after 48 h incubation in the 2D cell culture determined by MTT assay (n = 4).

down to *ca.* 60–70% at 200 μg mL^{-1} in all cell lines after 48 h (Fig. S5†). The increased cytotoxicity seen in Cet conjugated QDs agrees with the higher uptake of the particles by high-EGFR expressing SW480 cells (Fig. 2).

5FU conjugation in addition to ALA loading to Cet conjugated AS–2MPA (AS–2MPA–ALA–electrostatic–Cet–5FU) increased the cytotoxicity further in SW480 and HT29 cells (Fig. S6†): the viability of SW480 cells at 100 μg mL^{-1} [Ag] and *ca.* 30 μg mL^{-1} [5FU] was dropped to *ca.* 65% (Fig. S6a†). This indicates that an effective release of ester-linked 5FU from the EGFR targeting particles takes place and causes some toxicity, which should improve with the combination of PDT.

More than 90% of the healthy colon cells (CCD481) survived at high dosages of the QDs (200 μg Ag per mL and *ca.* 60 μg 5FU per mL) after 48 h incubation (Fig. S6c†), suggesting great potential of these QDs as chemo/phototherapy agents against cancer cells but not normal cells.

Intracellular PpIX generation in 2D and 3D cell cultures

Effective ALA-based PDT requires efficient conversion of the prodrug into the active photosensitiser PpIX.[61] Cells vary in their ALA-PpIX conversion efficiency due to differences in their metabolic activity, iron metabolism, the number of mitochondria, and enzyme levels.[62] The efficiency of SW480, HCT116, and HT29 cells to convert ALA to PpIX was first determined using free ALA as a function of ALA concentration (25–800 μM) and pro-drug incubation time (2–48 h). In all three cell lines, the mean fluorescence intensity of intracellular PpIX increased with ALA concentration up to a point (200–600 μM [ALA]), above which PpIX signal decreases, which may be due to enzyme saturation.[62,63] This trend and concentration range agree well with the literature.[63–66] Intracellular PpIX concentration also increased with the incubation time as expected.[64,65]

More importantly, a clear cell-type dependent difference in intracellular PpIX signal intensity was observed (Fig. 4a). SW480 cells are the most efficient, with the PpIX signal twice as strong as the signal observed in HT29 cells. PpIX generation by HCT116 was extremely poor. Hence, SW480 is not only an excellent cell line for selective delivery of ALA but also for its efficient conversion to PpIX.

Next, a similar study was performed with ALA loaded QD compositions between 0.17 and 0.7 mM [ALA] after short and long incubation times (4, 24 h) to elucidate the impact of EGFR targeting and the ALA loading chemistry on the intracellular PpIX level of the three CRC cells (Fig. 4b). The highest PpIX level was observed in SW480 cells at both incubation times, and AS–2MPA–ALA–electrostatic was determined as the most efficient QD in PpIX production. This is in line with the highly efficient ALA-PpIX conversion in SW480 cells demonstrated by free ALA (Fig. 4a) and the faster release of the prodrug from this conjugate with respect to covalently conjugated ones (Fig. 1d–f). The PpIX level of the SW480 cells

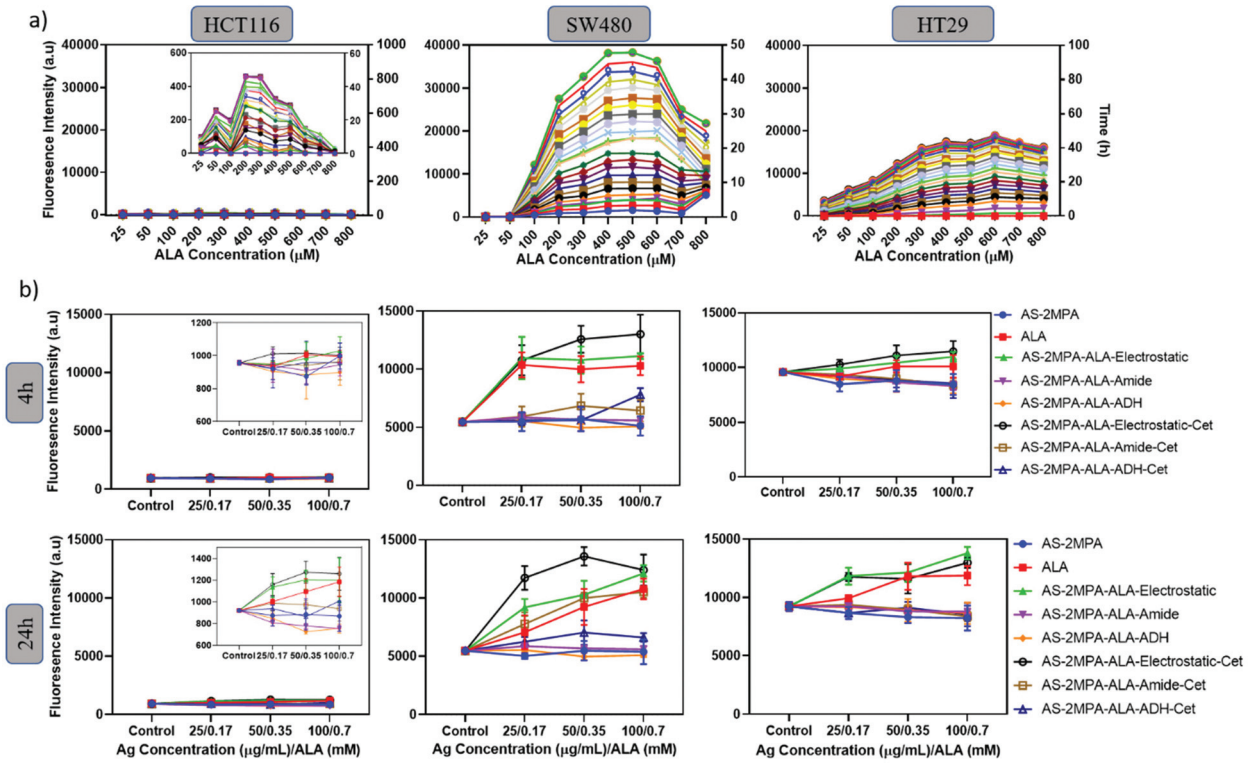

Fig. 4 (a) Intracellular formation of PpIX from free ALA in HCT116, SW480, and HT29 cells during 48 h incubation. Measurements were performed in 2 h intervals (n = 4). (b) Intracellular formation of PpIX in HCT116, SW480, and HT29 cells after 4 and 24 h incubation with free ALA or QD-conjugates (PpIX: λ_{exc}: 420 nm and λ_{em}: 635 nm).

increased further and significantly above the levels of free ALA after Cet conjugation, clearly demonstrating the benefit of EGFR targeting. The impact of Cet conjugation on QDs had a slight effect on intracellular PpIX levels of the treated HT29 cells due to low-EGFR expression. But QDs with electrostatically loaded ALA provided slightly better intracellular PpIX accumulation than free ALA in HT29 cells, as well. No significant levels of PpIX were achieved in HCT116 cells, as expected. Therefore, HCT116 was eliminated from the rest of the study.

Fluorescence microscopy confirmed an increasing level of PpIX in the SW480 cell line treated with AS–2MPA–ALA–electrostatic and AS–2MPA–ALA–electrostatic–Cet compared to free ALA (Fig. 5). The NIR optical signal detected in the CY8 channel confirmed QD internalisation which improved with Cet conjugation and PpIX generation. Besides, 5FU conjugation to these QDs did not cause a detectable change in the uptake or the PpIX production as can be visualised from the intensity of the signals in TRITC and CY8 channels.

In the 3D spheroids, QDs were incubated with the SW480 (for 4 and 24 h) and HT29 (for 24 h) cells to investigate further the cellular uptake and PpIX production in a more complex model. Bright fluorescence signals of the QDs (CY8 filter) and PpIX (TRITC filter) were observed in both SW480 and HT29 spheroids which indicated the successful intracellular uptake of QDs, ALA delivery and subsequent PpIX generation (Fig. S7†). Images also show that ALA was mainly taken up by the cancer cells rather than becoming bound in the collagen matrix, and much higher fluorescence was observed in the cancerous mass than in the surroundings. Control collagen spheroids without QD or its ALA conjugates showed no autofluorescence. As in the case of 2D cell cultures, high uptake of Cet-conjugated QDs was observed in SW480 spheroids even after 4 h and AS–2MPA–ALA–electrostatic–Cet provided the strongest PpIX signal. The intracellular PpIX level of HT29 3D-cultures was lower despite 24 h incubation due to the relatively poor/slow ALA-PpIX conversion efficiency of this cell line (Fig. 4 and Fig. S7†).

Cumulative data here point out that loading ALA to AS–2MPA QDs tagged with Cet improves the PpIX levels of the cells in an EGFR expression level-dependent manner depending on the efficiency of the cells to convert the prodrug to an active photosensitiser, and electrostatic loading of ALA is the most effective in delivery and release, facilitating the endogenous generation of high concentrations of PpIX.

ROS generation

Intracellular PpIX should produce ROS at toxic levels for an effective ALA-based PDT. SW480 and HT29 cells were treated with ALA, AS–2MPA–ALA, AS–2MPA–ALA–Cet, and AS–2MPA–ALA–Cet–5FU QDs at 100 μg mL^{-1} [Ag] dose (0.7 mM [ALA]) and were exposed to light irradiation. Typically, blue light is used for the FDA approved ALA (Levulan) prodrug, whereas most other indications, especially multimodal therapies, use red light.[33,66,67] Therefore, PDT studies were performed with two different light sources: (1) 420 nm blue lamp for 5 min and (2) 640 nm laser for 1 min. Then, ROS levels of the treated cells were measured from the green fluorescence intensity of ROS-oxidized 2′,7′-dichlorofluorescein (DCFH) (Fig. S8†). AS–2MPA did not produce any ROS by itself, confirming ALA as the sole photosensitiser if irradiated at these wavelengths. In general, fast ALA releasing AS–2MPA–ALA–electrostatic QDs produced more ROS than the covalently conjugated ones since it produced more PpIX (Fig. 1d–f and Fig. S8†). But, Cet conjugation increased the ROS levels of the cells treated with all QDs. Despite the low EGFR level of HT29, 24 h incubation allows significant QD internalisation by passive uptake (Fig. S4†). More efficient ALA-PpIX conversion of SW480 provided higher ROS levels than HT29 cells, which is best seen with electrostatically loaded ALA. Taken together, the nanocarriers can serve as promising photosensitising agents for PDT at both 420 nm and 640 nm.

PDT and PDT/chemotherapy combination in 2D cell cultures

The phototoxicity of the QD compositions was evaluated in 2D and 3D cell cultures. Cells were treated with QDs between 25 and 100 μg [Ag] per mL corresponding to 0.17–0.7 mM [ALA] for 4 h (SW480) and 24 h (SW480 and HT29). At these concentrations, no significant dark toxicity was observed. A short incubation time was not tested for HT29 due to lower uptake

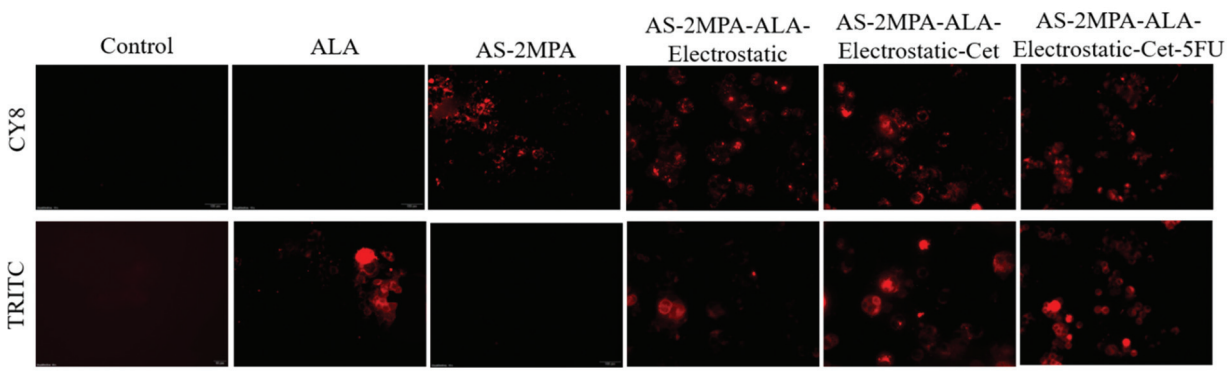

Fig. 5 Fluorescence imaging of intracellular PpIX (TRITC channel) and AS–2MPA (CY8 channel) signals of SW480 cells that were treated 24 h with ALA, AS–2MPA, AS–2MPA–ALA–electrostatic and AS–2MPA–ALA–electrostatic–5FU in the 2D cell culture. Treatment dose: 100 μg mL^{-1} [Ag]/0.7 mM [ALA]. Control: untreated cells. CY8 (λ_{exc}: 480 nm and λ_{em}: 810 nm) and TRITC (λ_{exc}: 545 nm and λ_{em}: 580–650 nm (band pass filter)).

and poorer ALA-PpIX conversion than SW480 cells. Treated cells were irradiated either with a blue lamp with the peak output at 420 nm for 5 min providing a fluence of 2.1 J cm^{-2} or with a 640 nm laser for 1 min, providing a fluence of 15.5 J cm^{-2}. No phototoxicity was observed on either cell line when only subjected to irradiation (light control) confirming that both illumination protocols are safe (Fig. 6 and 7). No toxicity was observed on cells treated with AS–2MPA + light, indicating that QDs do not cause phototoxicity in the absence of ALA. This is in agreement with the absence of ROS generation in the absence of ALA (Fig. S8†). Hence, any observed cytotoxicity will be related to ALA-PDT. Irradiation of cells treated with ALA or ALA loaded QDs showed incubation time, dose, cell type, ALA loading/conjugation chemistry, and irradiation wavelength-dependent phototoxicity.

Fig. 6 shows viability data following illumination using blue light. It is evident that both free ALA and AS–2MPA–ALA compositions elicited a higher phototoxic effect on SW480 cells than HT29 as expected based on better efficiency of the former to produce PpIX (Fig. 6). In general, QDs with electrostatically loaded ALA were the most effective, followed by the hydrazone and amide linked ones, respectively, parallel to the ALA release rate from these conjugates.

At short incubation times, the phototoxicity of free ALA was small with viabilities at and above 80% within the whole concentration range. Similarly, QDs with covalently conjugated ALA did not cause significant phototoxicity in SW480 cells after 4 h incubation, suggesting an insufficient level of ALA release and intracellular PpIX accumulation at short incubation time. However, QDs with electrostatically loaded ALA reduced the viability of this cell line to 53% at 0.35 mM ALA concentration after irradiation. This was reduced further to 43% when the particle was conjugated with Cet (AS–2MPA–ALA–Cet–electrostatic) and to 38% when 5FU (15 μg mL^{-1}) was conjugated as well, exhibiting a stronger therapeutic effect *via* EGFR targeted combination therapy. Considering that free 5FU reduced the viability to 71 and 52% at 10 and 25 μg mL^{-1} after 48 h incubation (Fig. S9†), these data show an apparent synergistic effect.

Phototoxicity increased dramatically using 24 h incubation of SW480 cells with the test materials. Free ALA caused about 40% reduction in viability at all concentrations, but the viability of AS–2MPA–ALA–electrostatic, AS–2MPA–ALA–ADH, and

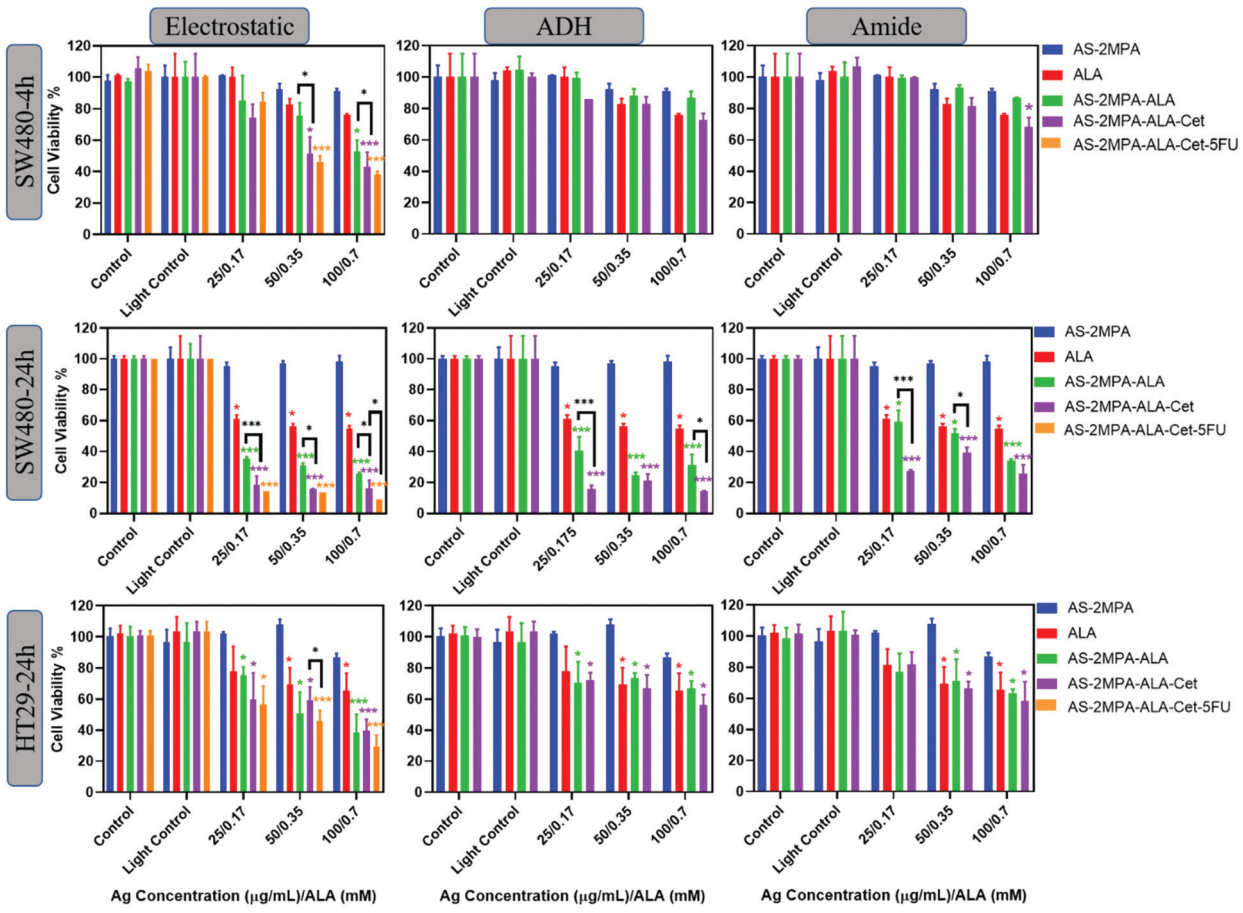

Fig. 6 Dose-dependent viability of SW480 (4 and 24 h incubation) and HT29 (24 h incubation) cells treated with ALA, AS–2MPA and QD-conjugates and exposed to 420 nm blue light for 5 min in the 2D cell culture. MTT assay was used for the determination of cell viability. 5FU concentrations in the studied range of AS–2MP–ALA–Cet–5FU were 7.5, 15.05 and 30.1 μg mL^{-1}. The controls shown are for cells without light exposure and light controls shown are exposed to light only. The data are expressed as mean ± S.D. (n = 4), (*p < 0.05, ***p < 0.001).

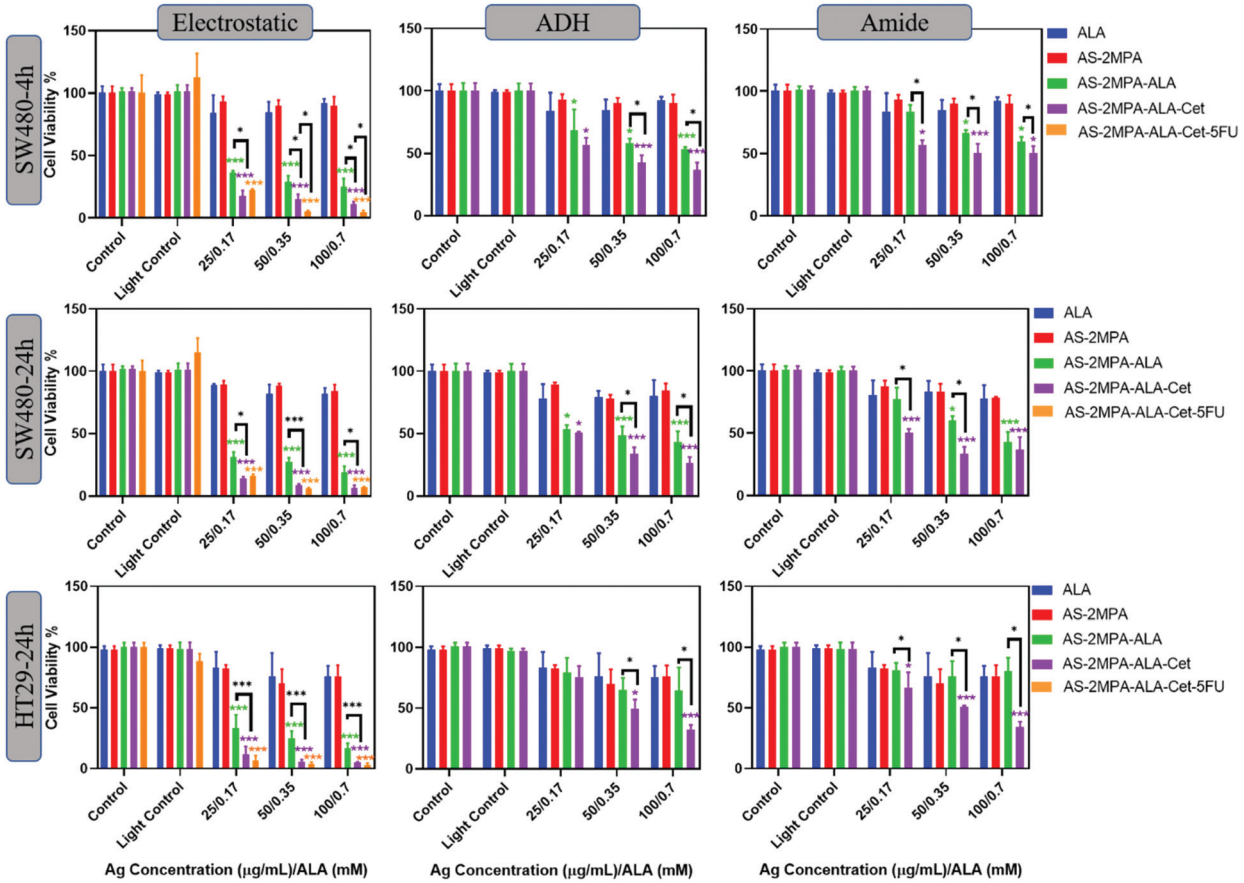

Fig. 7 Dose-dependent viability of SW480 (4 and 24 h incubation) and HT29 (24 h incubation) cells treated with ALA, AS–2MPA and QD-conjugates and 640 nm laser irradiation for 1 min in the 2D cell culture. MTT assay was used for the determination of cell viability. 5FU concentrations in the studied range of AS–2MP–ALA–Cet–5FU were 7.5, 15, 05 and 30.1 μg mL^{-1}. The controls shown are for cells without light exposure and light controls shown are exposed to light only. The data are expressed as mean ± S.D. (n = 4), (*p < 0.05, ***p < 0.001).

AS–2MPA–ALA–amide at 0.7 mM ALA dropped to 25, 31, and 35% (420 nm, 5 min), respectively. Indeed, even the lowest ALA concentration (0.17 mM) was below the IC_{50} if delivered by QDs, with the exception of the amide linked one. While some dose dependency in viability was observed with QDs bearing covalently linked ALA, no significant dose dependency was observed in AS–2MPA–ALA–electrostatic, due to quick ALA release providing sufficient PpIX and ROS for highly effective PDT within this concentration range. However, a clear benefit of Cet conjugation was observed at all doses and with all particles, with only 20% or less viability across the whole concentration range with electrostatic and ADH linked ALA, and 40% and below viability in the case of amide linked ALA. Targeted combination therapy reduced the viability of SW480 cells further to ~15% at the highest particle dose, with significantly better toxicity than targeted PDT monotherapy, suggesting critical antiproliferative activity in addition to ALA-based PDT. At lower doses, the concentration of 5FU may not be sufficient to observe its effect on viability in 24 h incubation.[68,69]

In the case of HT29 cells, only the QDs with electrostatically loaded ALA provided higher phototoxicity than free ALA since this cell line requires a higher concentration of ALA to reach an effective intracellular PpIX concentration at the same incubation time. Since its EGFR expression is not high, a significant advantage of Cet conjugation was not observed. Viability of the HT29 cells treated with free ALA + 420 nm light was between ~80 and 65% and dropped down to ~60–40% with AS–2MPA–ALA–electrostatic–Cet + 420 nm irradiation in the studied concentration range. Better toxicity was observed again with the combination therapy, especially at mid- and high-doses (15 and 30 μg 5FU per mL) with ~30% viability at the highest dose. Free 5FU reaches IC_{50} at about 10 and 25 μg mL^{-1} only after 48 h incubation in HT29 and SW480 cells, respectively (Fig. S9†), clearly demonstrating the benefit of targeted combination therapy.

Red light is commonly used for ALA-PDT owing to the deeper penetration into tissue, and several studies have demonstrated ALA-based PDT using different red light sources such as lamps, LEDs, or lasers.[21,70,71] Fig. 7 shows viability of cells treated with the conjugates at the same concentration followed by red light irradiation by a 640 nm laser (15.5 J cm^{-2}), which is close to the longest wavelength Q-band absorption peak of PpIX. Again, no phototoxicity from AS–2MPA but significant phototoxicity of ALA and AS–2MPA–ALA compositions

was observed. According to Wawrzyniec *et al.* SW480 cells treated with 0.5 mM ALA at 10 and 30 J cm^{-2} (600–720 nm) maintained a viability around 85% which is comparable to the free ALA toxicity seen here, after 640 nm irradiation.[70,72]

As shown in Fig. 7, using a 4 h incubation followed by 640 nm irradiation of the cells treated with AS–2MPA–ALA–electrostatic and AS–2MPA–ALA–electrostatic–Cet QDs reduced the viability of SW480 cells below 40% even at the lowest concentration, indicating strong phototoxicity generated at 640 nm reaching 11% with Cet conjunction at 0.7 mM [ALA]. On the other hand, free ALA + 640 nm irradiation reduced the viability to about 80%. Loading of ALA (0.1 mM) to PEGylated chitosan doubled the toxicity in the CT26 CRC cell line after irradiation with a 635 nm LED.[73] Compared to this example, a stronger enhancement over ALA-phototoxicity was observed with ALA delivered by QDs and even more with Cet conjugation, confirming the design's success. Combination therapy increased the toxicity further, almost to the level of complete loss of viability even after 4 h incubation at 15–30 μg mL^{-1} 5FU/0.35–0.7 mM [ALA] concentration. Enhanced phototoxicity over free ALA was also observed under the same conditions (4 h + 640 nm) with AS–2MPA–ALA–ADH, and AS–2MPA–ALA–amide, as well, while they were not so effective at 420 nm irradiation. They have also displayed improved phototoxicity when conjugated with Cet reaching IC50 and below at and above 0.35 mM ALA concentration.

In the case of HT29 cells, a more pronounced therapeutic outcome was observed under 640 nm irradiation, including the amide and hydrazone conjugates. Cet conjugated QDs with covalently linked ALA caused more than 50% loss of viability at and above 0.350 mM ALA. All QD compositions with electrostatically loaded ALA caused more than 60% reduction in viability, reaching almost complete loss of viability with Cet conjugation and combination therapy at all concentrations. At the lowest concentration, combination therapy seems to improve the toxicity over the PDT-monotherapy more significantly, since at higher doses PDT already caused dramatic toxicity by itself. This level of toxicity is quite encouraging for CRC. The most relevant study on ALA-PDT of the HT29 cell line reported about 50% cell killing at 1 mM ALA concentration with blue light irradiation and about 20% with red light at 3 J cm^{-2} using LEDs[30] which provided 88% tumour inhibition after three treatments of 250 mg ALA per kg-blue light irradiation (32 J cm^{-2}). Therefore, targeted ALA-based PDT and its combination with 5FU successfully enhanced killing of CRC cells, providing great hope for better treatment of CRC.

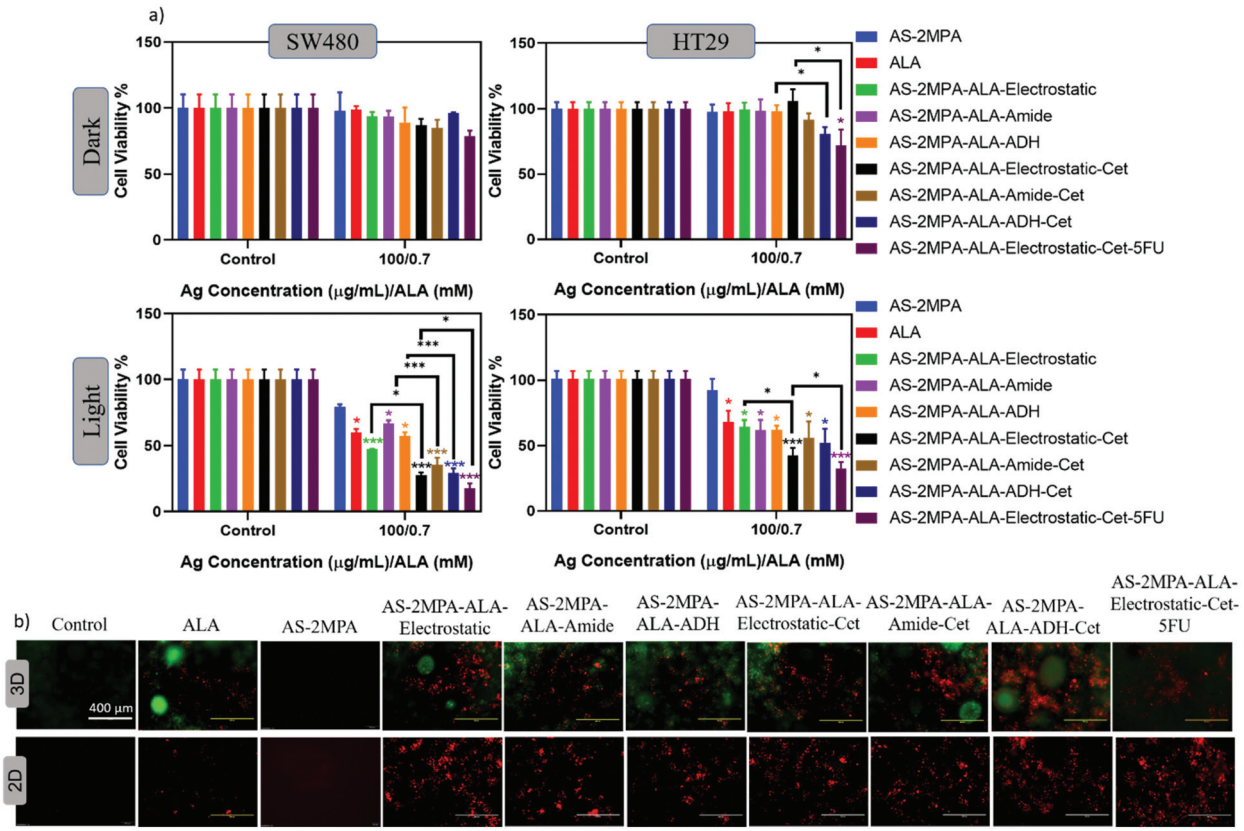

Fig. 8 (a) Viability of cells in SW480 and HT29 3D spheroids treated with free ALA, AS–2MPA or QD-conjugates at 100 μg mL^{-1} [Ag] dose for 24 h and illuminated at 420 nm for 5 min. Viability was determined by Alamar blue assay. The data are expressed as mean ± S.D. (n = 3), (*p < 0.05, ***p < 0.001). (b) Apoptosis fluorescence imaging assay of SW480 cells in 2D and 3D spheroids stained with Annexin V-FITC/PI after being treated 24 h with free ALA, AS–2MPA or QD-conjugates at 100 μg mL^{-1} [Ag] dose and irradiated for 5 min at 420 nm.

PDT and PDT/chemotherapy combination in 3D cell cultures

Prompted by the efficacy of the QD nanocarriers in the 2D cell cultures, we also investigated their PDT efficacy on 3D spheroids grown in compressed collagen scaffolds. Improvement of cell organisation, enhancement of expression of differentiated functions, multicellular resistance, and limited drug penetration are some advantages of using 3D models over 2D cell culture.[74,75] Therefore, 3D models provide a more representative model for determining the therapeutic response *in vitro*. Since the absorbance-based MTT assay is not suitable to check viability in light scattering 3D cell cultures, the fluorescence-based Alamar blue assay was used to determine the viability of cells before and after PDT in 3D spheroids. The 3D spheroid models were incubated with all QD groups at 100 μg mL^{-1} [Ag] dose for 24 h and then irradiated with 420 nm blue light for 5 min. A large reduction in cell viability was observed in both SW480 and HT29 3D spheroids after light irradiation (Fig. 8a). Viability of SW480 cells in spheroids treated with free ALA, AS–2MPA–ALA–electrostatic, AS–2MPA–ALA–ADH, and AS–2MPA–ALA–amide were 93–96% in the dark but was reduced to 59, 47, 67 and 57% after PDT treatment. Electrostatically loaded ALA was again most efficient and better than free ALA in agreement with data obtained by 2D cell cultures. When QDs were directed to cells with Cet conjugation, all QDs were significantly more effective than free ALA, and the live-cell fraction was only 28, 29, and 35%, for the electrostatically loaded, ADH, and amide linked conjugates, respectively. In HT29 3D spheroids, AS–2MPA–ALA did not show a clear advantage over free ALA, but Cet conjugated QDs triggered a greater cell killing and more effective PDT with 42, 52, and 56% viable cell count when treated with electrostatically loaded, ADH, and amide conjugated QDs, respectively.

In both 3D spheroids, combination therapy (targeted chemo/PDT) almost doubled the toxicity over targeted PDT monotherapy, and the viability was reduced to 18 and 32% in SW480 and HT29 spheroids, respectively. All trends are in agreement with 2D data. But in general, toxicity was lower in 3D spheroids, which is possibly due to higher chemo/phototherapy resistance of spheroids.[76]

Determination of apoptotic cell death

Based on observed toxicity of the targeted PDT *via* ALA delivering QDs and the targeted combination therapy in SW480 2D cell cultures and 3D spheroids, contribution of apoptotic/necrotic cell death in these therapeutic approaches was studied using Annexin V-FITC/PI co-staining assay. Cells were treated with QDs at 100 μg mL^{-1} [Ag] for 24 h and then were irradiated at 420 nm (5 min) (Fig. 8b). Apoptotic cells were

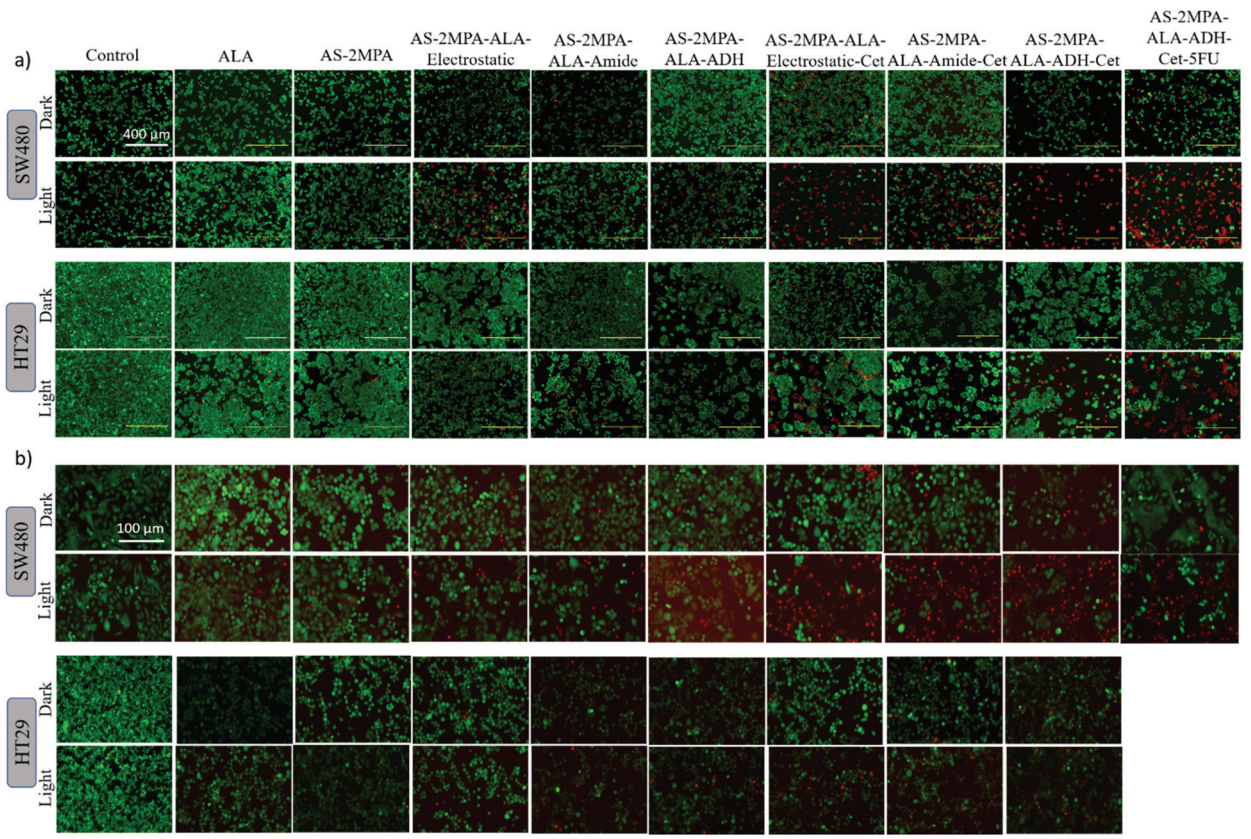

Fig. 9 Live/dead assay fluorescence images of Calcein-AM/propidium iodide (PI) stained (live: green/dead: red) SW480 and HT29 cells in 2D cultures that were treated for 4 h with free ALA, AS–2MPA or QD-conjugates at 100 μg mL^{-1} [Ag] and irradiated (a) at 420 nm with a blue lamp for 5 min and (b) with a 640 nm laser for 1 min. Dark: no light exposure.

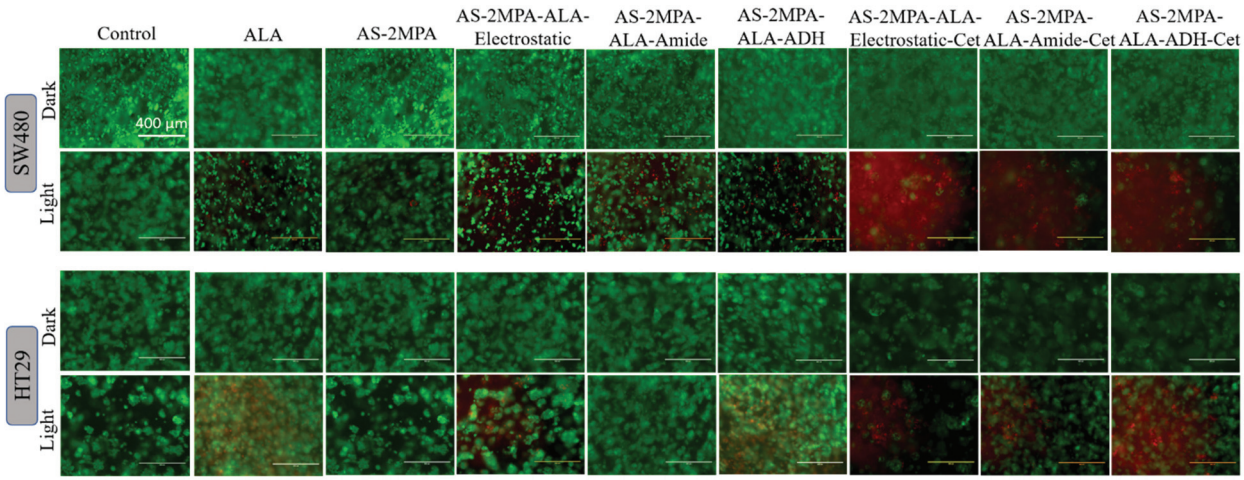

Fig. 10 Live/dead assay fluorescence images of Calcein-AM/propidium iodide (PI) stained (live: green/dead: red) SW480 and HT29 3D spheroids that were treated for 4 h with free ALA, AS–2MPA or QD-conjugates at 100 μg mL^{-1} [Ag] and 5 min light irradiation with a 420 nm blue lamp. Dark: no light exposure.

indicated with green fluorescence, and cells that lost cell membrane integrity showed red fluorescence.

Accordingly, cells treated with either free ALA or QD conjugates mostly have red luminescence suggesting late apoptotic/necrotic cell death and QD conjugates were more effective than free ALA in 2D cell cultures. In 3D spheroids mostly apoptotic cells were observed with an increasing amount of late apoptotic/necrotic cells with Cet conjugated QDs. Hence, in both 2D and 3D, a clear advantage of targeted delivery of ALA to CRC cells and combination therapy in driving cells to apoptotic/necrotic cell death was observed.

Live/dead fluorescence imaging in 2D and 3D culture: confirmation of cell death

The high toxicity of PDT and PDT/chemo combination observed in 2D and 3D culture was further confirmed with live/dead assays using Calcein-AM/propidium iodide (PI) co-staining. This study was performed after 4 h incubation of the cells with the test materials to highlight the clear benefit of targeting and observe differences based on the cell type and conjugation chemistry. In the absence of laser, none of the reagents caused a significant cell death, and in the absence of ALA, no photo-damage was observed at 420 nm or 640 nm in neither 2D nor 3D models since all these cells showed a vivid green fluorescence indicating live cells (Fig. 9 and 10). This confirms that any dead cell population observed in all other cases is due to PDT and combination therapy. As seen in Fig. 9, a significant population of dead cells (red fluorescence) was observed in SW480 cells in 2D cell culture when ALA was delivered with Cet conjugated QDs, while cells treated with free ALA show mostly green fluorescence from live cells. Besides, the greatest cell killing was observed with EGFR targeting QDs delivering both ALA and 5FU, in agreement with viability assays and highlighting the superiority of both targeting and combination therapy over monotherapy. In HT29 cells, only AS–2MPA–ALA–Cet and AS–2MPA–ALA–ADH–Cet provided a noticeable dead cell population, while the combination therapy was the most successful approach again to achieve an appreciable cell killing.

Imaging of the 3D spheroids was more challenging since focusing in turbid specimens is more difficult (Fig. 10). But overall, significant concentrations of dead cells (red fluorescence) were observed in spheroids treated with the Cet conjugated particles, especially with the electrostatically loaded or hydrazone linked ALA, and more in SW480 spheroids, as in the case of 2D cell cultures. Also, the combination therapy showed a clear benefit in both cell lines.

Conclusion

In this study, AS–2MPA QDs with NIR emission were adapted as theranostic agents for targeted ALA-PDT and chemotherapy combination treatment of EGFR(+) colorectal cancer (CRC). AS–2MPA QDs were conjugated with Cetuximab to deliver the ALA to EGFR(+) CRC cells to improve the bioavailability and accumulation of ALA in targeted cancer cells for enhancing intracellular generation of the metabolised photosensitiser PpIX and the therapeutic outcome of PDT. ALA was loaded to QDs in three different ways to trigger its release *via* different stimulants. In a further refinement, the chemotherapeutic agent 5FU was also conjugated to the QDs for tumour targeted chemotherapy/PDT combination treatment to improve the therapeutic outcome further. All the QD conjugates emit strongly around 830 nm and have small sizes, ideal for *in vivo* deep-tissue imaging and molecular targeting.

The *in vitro* studies performed in 2D and 3D cell cultures demonstrate expression level dependent EGFR targeting of the AS–2MPA–ALA–Cet QDs in three CRC cell lines (SW480 > HCT116 > HT29) and strong intracellular NIR signals with good contrast with the background. Viability studies following

48 h incubation demonstrated very low or insignificant levels of dark toxicity.

Three different techniques for ALA loading onto the QDs were compared: electrostatic binding, covalent conjugation *via* amide and hydrazone linkages. ALA was released from the electrostatically loaded QDs faster, but importantly, all three loading methods elicited a higher rate of ALA release at acidic pH than physiological pH, favouring ALA release in the more acidic tumour microenvironment, and intracellular lysosomal release following endocytic uptake of the QDs. Faster release of ALA from electrostatically loaded particles also caused faster PpIX accumulation in the cancer cell lines in both 2D and 3D cell cultures of the CRC cells, especially at short incubation times. However, these cell lines differ significantly in ALA-PpIX conversion efficiency in decreasing order of SW480 > HT29 > HCT116, suggesting that SW480 would be more susceptible to ALA-based PDT. Besides, intracellular PpIX levels of the cells increased with incubation time and the ALA concentration, with the highest efficiency in the 200–600 mM range. Irradiation of cells treated with QDs, ALA or the ALA loaded QDs was performed both with a blue lamp at 420 nm and a coherent laser at 640 nm, corresponding to the Soret band absorbance and the longest wavelength absorption of PpIX, respectively.

Highest PpIX levels and therefore ROS generation were observed in SW480 cells using AS–2MPA–ALA–electrostatic–Cet conjugates due to higher cellular uptake by strong EGFR over-expressing SW480, faster ALA release than covalently conjugated ALA, especially at acidic pH, and efficient ALA-PpIX conversion. This was translated into high phototoxicity in SW480 cell lines even after 4 h incubation with ALA concentration as low as 0.35 mM after 5 min – 420 nm irradiation and 0.17 mM ALA-1 min – 640 nm irradiation, with less than 50 and 20% viable cell count, respectively. Cells treated in the same way but with free ALA maintained 80% viability at 0.17–0.7 mM [ALA] while after conjugation of ALA to untargeted QDs (AS–2MPA–ALA) the viability further reduced to 30–60% at 0.7 mM [ALA] after PDT. The use of a longer incubation time (24 h) allows more particle uptake and higher ALA delivery levels to cells thereby enhancing the phototoxicity particularly in SW480 cells. Although HT29 was more challenging to treat due to poor ALA-PpIX conversion efficiency and the low EGFR expression level, irradiation at 420 nm after 24 h incubation with AS–2MPA–ALA–Cet–electrostatic at 0.7 mM [ALA] resulted in 60% loss in the viable cell count and caused almost complete loss of viability after 640 nm irradiation.

In the case of the amide and hydrazone linked ALA, although the response is somewhat slower than electrostatically loaded ALA, significantly better toxicity than free ALA was achieved with EGFR targeting QDs especially after longer incubation time to allow hydrolysis of the covalent bonds and irradiation at 640 nm with the diode laser.

Despite the highly successful ALA-PDT monotherapy at low ALA concentrations, targeted combination therapy was also studied but only with the fast ALA releasing electrostatically ALA loaded QDs. Use of AS–2MPA–ALA–Cet–5FU QDs + photo-irradiation enhanced toxicity even further and eliminated almost all cells at and above 0.35 mM ALA/15 μg mL^{-1} 5FU doses, which is dramatically lower than IC50 of each component. Successful therapy of CRC cells was also confirmed at 0.7 mM [ALA] after 24 h incubation of all QDs in 3D spheroids of the cells, which is a more complex structure. In particular, AS–2MPA–ALA–Cet–5FU reduced the cell viability of 3D SW480 spheroids almost 2-fold compared to PDT-monotherapy after 420 nm irradiation and reduced the viability to 18% in SW480 and 32% in HT29. The reduction in the viable cell count was confirmed as apoptotic/necrotic cell death in both 2D and 3D cultures.

Although further *in vivo* validation is required, these particles are expected to enhance tumour accumulation *in vivo via* multilevel targeting: firstly, active tumour targeting *via* over-expression of EGFR, and secondly passive tumour targeting owing to the EPR effect that favours higher retention of nanoparticles in tumours *versus* normal adjacent tissue. Rapidly dividing cells, such as tumour cells, provide more efficient conversion of ALA to PpIX, which also confers some further PDT selectivity *in vivo*. Finally, fast release in the acidic tumour microenvironment could further augment selectivity of the treatment. Therefore, in principle there are four mechanisms that could confer selective PDT of tumours with these QDs.

Overall, evidence provided in both 2D and 3D cell cultures confirms that the cell surface receptor targeted AS–2MPA–ALA–Cet QDs can improve the success of ALA-PDT of CRC based on higher accumulation of ALA at selected tumour cells and stronger phototoxicity with a 640 nm diode laser. Combination of targeted PDT/5FU treatment *via* use of AS–2MPA–ALA–Cet–5FU nanoparticles provides a highly selective, local, and effective therapy coupled with NIR image guidance; therefore this approach provides a new and highly effective theranostic method for the treatment of EGFR(+) CRC. Although these theranostic nanoparticles were tested on EGFR (+) CRC cells, they can also be adapted for different tumour types, different receptors and chemotherapy combinations.

Author contributions

All authors have given approval to the final version of the manuscript.

Conflicts of interest

The author(s) declare that they have no competing interests.

Acknowledgements

The authors would like to thank Dr Gülsu Şimşek for help on the preparation of ICP-MS, respectively. This work was supported partly through the Newton-Katip Çelebi Fund (British Council and TUBITAK grant codes: GA 334995, TUBITAK grant code: 216Z131).

References

1 J. Chen, X. Chen, Z. Yang, X. Tan, J. Wang and Y. Chen, *J. Biomed. Mater. Res., Part A*, 2018, 319.
2 Y. Shih, T. Luo and P. Chiang, *J. Controlled Release*, 2017, **258**, 196.
3 A. Marta, B. D. Blanco and C. Gomez, *Photodiagn. Photodyn. Ther.*, 2015, **12**(3), 446.
4 J. Chen, C. Ning and Z. Zhou, *Prog. Mater. Sci.*, 2017, **99**, 1.
5 Y. Wang, M. Yang and J. Qian, *Carbohydr. Polym.*, 2019, **203**, 203.
6 T. Dougherty and S. Schwartz, *Nat. Rev. Cancer*, 2003, **3**, 380.
7 G. Obaid, M. Broekgaarden and A. Bulin, *Nanoscale*, 2016, **8**(25), 12471.
8 S. Mordon and C. Frochot, *Porphyrin Science by Women: In 3 Volumes*, 2019, vol. 3, p. 28.
9 P. De Silva, M. A. Saad, H. C. Thomsen, S. Bano, S. Ashraf and T. Hasan, *J. Porphyrins Phthalocyanines*, 2020, **24**, 1320.
10 C. Jiang, H. Cheng, A. Yuan, X. Tang, J. Wu and Y. Hu, *Acta Biomater.*, 2015, **14**, 61.
11 M. Tanaka, H. Kataoka and M. Mabuchi, *Anticancer Res.*, 2011, **770**, 763.
12 L. B. Rocha, F. Schaberle, J. M. Dabrowski, S. Simões and L. G. Arnaut, *Int. J. Mol. Sci.*, 2015, **16**, 29236.
13 C. Chung, K. Chung, Y. Jeong and D. H. Kang, *Int. J. Nanomed.*, 2013, **8**, 809.
14 R. W. K. Wu, E. S. M. Chu, Z. Huang, M. C. Olivo, D. C. W. Ip and C. M. N. Yow, *J. Innov. Opt. Health Sci.*, 2015, **8**, 1.
15 B. O. Sun, W. E. I. Li and N. Liu, *Oncol. Lett.*, 2016, **11**, 2071.
16 M.-H. Chang, C.-L. Pai, Y.-C. Chen, H.-P. Yu, C.-Y. Hsu and P.-S. Lai, *Nanomaterials*, 2018, **8**, 121.
17 C. A. Kruger and H. Abrahamse, Targeted Photodynamic Therapy as Potential Treatment Modality for the Eradication of Colon Cancer, Multidisciplinary Approach for Colorectal Cancer, Keun-Yeong Jeong, *IntechOpen*, 2019.
18 M. Chang, C. Pai, Y. Chen, H. Yu, C. Hsu and P. S. Lai, *Nanomaterials*, 2018, **8**, 121.
19 A. Di Martino, A. Pavelkova, P. S. Postnikov and V. Sedlarik, *J. Photochem. Photobiol., B*, 2017, **175**, 226.
20 B. Krammer and K. Plaetzer, *Photochem. Photobiol. Sci.*, 2008, **7**, 283.
21 A. Punjabi, W. Xiang, T. Amira, M. El-Rifai, L. Hyungseok, Z. Yuanwei, W. Chao, Z. Liu, A. M. Chan, C. Duan and G. Han, *ACS Nano*, 2014, **8**, 10621.
22 K. M. Tewari and I. M. Eggleston, *Photochem. Photobiol. Sci.*, 2018, **17**, 1553.
23 H. Xu, C. Liu, J. Mei, C. Yao, S. Wang, J. Wang, Z. Li and Z. Zhang, *Int. J. Nanomed.*, 2012, **7**, 5029.
24 K. Mahmoudi, K. L. Garvey, A. Bouras, G. Cramer, H. Stepp, J. G. Jesu Raj, D. Bozec, T. M. Busch and C. G. Hadjipanayis, *J. Neuro-Oncol.*, 2019, **141**, 595.
25 Z. Malik, *Photonics & Lasers in Medicine*, 2015, **4**, 19.
26 R. F. Donnelly, P. A. Mccarron and A. D. Woolfson, *Perspect. Med. Chem.*, 2007, **44**, 49–63.
27 R. F. V. Lopez, N. Lange, R. Guy and M. V. L. B. Bentley, *Adv. Drug Deliv. Rev.*, 2004, **56**, 77.
28 H. Xu, C. Liu, J. Mei, C. Yao, S. Wang, J. Wang, Z. Li and Z. Zhang, *Int. J. Nanomed.*, 2012, **7**, 5029.
29 K. Wawrzyniec, A. Kawczyk-krupka, Z. P. Czuba, W. Król and A. Sieroń, *Photodiagnosis Photodyn. Ther.*, 2015, **12**, 598.
30 T. Hatakeyama, Y. Murayama, S. Komatsu and A. Shiozaki, *Oncol. Rep.*, 2013, **29**, 911.
31 X. Shi, H. Zhang, W. Jin, W. Liu, H. Yin and Y. Li, *J. Photochem. Photobiol., B*, 2019, **198**, 111586.
32 H. Masuda, M. Kimura, A. Nishioka and H. Kato, *J. Dermatol. Sci.*, 2019, **93**, 109.
33 J. L. Mccullough, G. D. Weinstein, R. Kaplan, S. D. Glazer and J. R. Taylor, *J. Am. Acad. Dermatol.*, 2001, **45**, 96.
34 Y. Mir, S. A. Elrington and T. Hasan, *Nanomedicine*, 2013, **9**, 1114.
35 G. Obaid, I. Chambrier, M. J. Cook and D. A. Russell, *Photochem. Photobiol. Sci.*, 2015, **14**, 737.
36 F. Wen and Q. Li, *World J. Gastroenterol.*, 2016, **22**, 5332.
37 C. Messa, F. Russo and M. G. Caruso, *Acta Oncol.*, 1998, **37**, 284.
38 S. Maya, B. Sarmento, V. K. Lakshmanan, D. Menon and R. Jayakumar, *J. Biomed. Nanotechnol.*, 2014, **10**, 1416.
39 P. Pfeiffer, D. Nielsen, J. Bjerregaard, C. Qvortrup, M. Yilmaz and B. Jensen, *Ann. Oncol.*, 2008, **19**, 1141.
40 S. Qin, Y. Li, L. Wang, J. Xu, Y. Cheng, Y. Bai, W. Li, N. Xu, L. Z. Lin, Q. Wu, Y. Li, J. Yang, H. Pan, X. Ouyang, W. Qiı, K. Wu, J. Xiong, G. Dai, H. Liang, C. Hu, J. Zhang, M. Tao, Q. Yao, J. Wang, S. P. Eggleton and T Liu, *J. Clin. Oncol.*, 2018, **36**, 3031.
41 M. Hashemkhani, K. Bilici, A. Muti, A. Sennaroglu and H. Yagci, *New J. Chem.*, 2020, **44**, 5419.
42 I. Hocaoglu, M. N. Çizmeciyan and R. Erdem, *J. Mater. Chem.*, 2012, **22**, 14674.
43 F. Hu, C. Li, Y. Zhang, M. Wang, D. Wu and Q. Wang, *Nano Res.*, 2015, **8**, 1637.
44 D. Aydemir, M. Hashemkhani, E. G. Durmusoglu, H. Y. Acar and N. N. Ulusu, *Talanta*, 2019, **194**, 501–506.
45 M. Hashemkhani, A. Muti, A. Sennaroglu and H. Yagci, *J. Photochem. Photobiol., B*, 2020, **213**, 112082.
46 C. G. Hadjipanayis, G. Widhalm and W. Stummer, *Neurosurgery*, 2015, **77**, 663.
47 K. Mahmoudi, K. L. Garvey, A. Bouras, G. Cramer, H. Stepp, J. G. Jesu Raj, D. Bozec, T. M. Busch and C. G. Hadjipanayis, *J. Neuro-Oncol.*, 2019, **141**, 595.
48 T. Picart, M. Berhouma, C. Dumot, J. Pallud, P. Metellus and X. Armoiry, *Neurochirurgie*, 2019, **65**, 164.
49 J. D. Predina, J. Runge and A. Newton, *Sci. Rep.*, 2019, **9**, 1.
50 D. Ozkan, S. Aydin, I. Hocaoglu, F. Havva, Y. Acar and N. Basaran, *Chem.-Biol. Interact.*, 2018, **291**, 212.
51 I. Hocaoglu, D. Asik and G. Ulusoy, *Colloids Surf., B*, 2015, **133**, 198.
52 K. Shigeta, T. Hayashida, Y. Hoshino, K. Okabayashi, T. Endo and Y. Ishii, *PLoS One*, 2013, **8**(6), e66302.
53 L. M. Hadi, E. Yaghini and A. J. Macrobert, *Int. J. Mol. Sci.*, 2020, **21**(9), 3203.

54 L. Ouyang, D. He and J. Zhang, *Bioorg. Med. Chem.*, 2011, **19**(12), 3750.
55 L. E. Brus, *J. Chem. Phys.*, 1984, **80**(9), 4403.
56 L. M. Hadi, E. Yaghini, K. Stamati, M. Loizidou and A. J. Macrobert, *Acta Biomater.*, 2018, **81**, 80–92.
57 A. Sangtani, E. Petryayeva, M. Wu, *et al.*, *Bioconjugate Chem.*, 2018, **29**(1), 136.
58 C. F. Zhu, S. Battah, X. Kong, B. J. Reeder, R. C. Hider and T. Zhou, *Bioorg. Med. Chem. Lett.*, 2015, **25**(3), 558.
59 M. Sousa De Almeida, E. Susnik, B. Drasler, P. Taladriz-Blanco, A. Petri-Fink and B. Rothen-Rutishauser, *Chem. Soc. Rev.*, 2021, **50**(9), 5397.
60 A. M. Master and A. S. Gupta, *Nanomedicine*, 2012, **7**(12), 1895–1906.
61 M. Kaliszewski, A. Juzeniene and P. Juzenas, *Photodiagnosis Photodyn. Ther.*, 2005, **2**(2), 129.
62 A. de Souza, K. Marra, J. Gunn, K. S. Samkoe, S. C. Kanick, S. C. Davis, M. S. Chapman, E. V. Maytin, T. Hasan and B. W. Pogue, *Br. J. Cancer*, 2016, **115**(7), 805.
63 A. Casas, H. Fukuda, V. G. Di and A. Batlle, *Br. J. Cancer*, 2001, **85**(2), 279.
64 C. S. Betz, J. Lai and W. Xiang, *Photochem. Photobiol. Sci.*, 2019, **1**(5), 315.
65 L. Anayo, A. Magnussen, A. Perry, M. Wood and A. Curnow, *Lasers Surg. Med.*, 2018, **50**(5), 552.
66 E. W. B. Jeffes, *J. Dermatol. Treat.*, 2002, **13**(1), S19.
67 B. Osiecka, K. Jurczyszyn and P. Ziółkowski, *Med Sci. Monit.*, 2012, **18**(2), 15–19.
68 C. S. Wong, V. W. Wong and C. M. Chan, *Oncol. Rep.*, 2008, **20**(1), 89.
69 F. G. Pruefer, F. Lizarraga, V. Maldonado and J. Melendez-Zajgla, *J. Chemother.*, 2008, **20**(3), 348.
70 K. Wawrzyniec, A. Kawczyk-Krupka, Z. P. Czuba, W. Krol and A. Sieron, *Photodiagn. Photodyn. Ther.*, 2015, **12**(4), 598.
71 C. D. Enk and A. Levi, *Photodermatol., Photoimmunol. Photomed.*, 2012, **28**(6), 332.
72 J. Yuri, N. Hioka and E. Kimura, *Photodiagnosis Photodyn. Ther.*, 2012, **9**(2), 122.
73 C. Chung, K. Chung, Y. Jeong and D. H. Kang, *Int. J. Nanomed.*, 2013, **8**, 809.
74 Z. L. Zhou, J. Liu, J. Huang, T. W Rees, Y Wang, H. Wang, X. Li, H. Chao and P. J. Stang, *Proc. Natl. Acad. Sci. U. S. A.*, 2019, **116**(41), 20296.
75 L. Mohammad-hadi, A. J. Macrobert, M Loizidou and E. Yaghini, *Nanoscale*, 2018, **10**, 1570.
76 B. Yang, H. Liu, H. Yang, W. Chen, J. Wu, X. Feng, R. Tong, H. Yu, Y. Chen, Z. Lv, W. Sun, B. He, J. Wu, G. Yu, Z. Mao and S. Zheng, *J. Mater. Chem. B*, 2019, **7**(42), 6476.